

Effect of stress history on sediment transport and channel adjustment in graded gravel-bed rivers

Chenge An^{1,2}, Marwan A. Hassan², Carles Ferrer-Boix³, Xudong Fu¹

¹ Department of Hydraulic Engineering, State Key Laboratory of Hydrosience and Engineering, Tsinghua University, Beijing, China.

² Department of Geography, The University of British Columbia, Vancouver, BC, Canada.

³ ~~Serra Húnter Fellow~~, Department of ~~Graphic and Design Engineering~~~~Civil and Environmental Engineering~~, Technical University of Catalonia, Barcelona, Spain.

Correspondence to: Xudong Fu (xdfu@tsinghua.edu.cn)

Abstract. With the increasing attention on environmental flow management for the maintenance of habitat diversity and ecosystem health of mountain gravel-bed rivers, much interest has been paid to how inter-flood low flow can affect gravel-bed river morphodynamics during subsequent flood events. Previous research has found that antecedent conditioning flow can lead to an increase in the critical shear stress and a reduction in sediment transport rate during a subsequent flood. But how long this effect can last during the flood event has not been fully discussed. In this paper, a series of flume experiments with various durations of conditioning flow are presented to study this problem. Results show that channel morphology adjusts significantly within the first 15 minutes of the conditioning flow, but becomes rather stable during the remainder of the conditioning flow. The implementation of conditioning flow can indeed lead to a reduction of sediment transport rate during the subsequent hydrograph, but such effect is limited only within a relatively short time at the beginning of the hydrograph. This indicates that bed reorganization during the conditioning phase, which induce the stress history effect, is likely to be erased with increasing intensity of flow and sediment transport during the subsequent flood event.

1 Introduction

Prediction of sediment transport is of vital importance because it is related to many aspects of river dynamics and management, including river morphodynamics modeling (Parker, 2004), river restoration (Chin et al., 2009), aquatic habitats (Montgomery et al., 1996), natural hazard planning (Marston, 2008), bedrock erosion (Sklar and Dietrich, 2004), and landscape evolution (Howard, 1994). In ~~mountain~~ gravel-bed rivers, sediment transport is controlled by flow magnitude and flashiness, sediment supply, bed surface structures, channel morphology and the grain size distribution (GSD) of sediment (Montgomery and Buffington, 1997; [Masteller et al., 2019](#)). Therefore, prediction of sediment transport in mountain rivers still remains difficult despite the large body of existing theories. This is due to the fact that these theories were mostly developed for lowland streams with continuous sediment supply and an average flow regime, which do not apply to mountain streams (Gomez and Church, 1989; Rickenmann, 2001; Schneider et al., 2015).

31 For example, the hydrograph of mountain gravel-bed rivers is often characterized by large fluctuations of flow
32 discharge, including both short-term flash flood and long-term inter-flood low flow (Powell et al., 1999). However, research
33 on the morphodynamics of mountain rivers often focuses on the effects of floods (or constant high flow) and neglects the role
34 of inter-flood low flow, with the consideration that most sediment transport and morphological adjustments of mountain rivers
35 occur during relatively high flows (Klingeman and Emmett, 1982; Paola et al., 1992).

36 Reid and colleagues (Reid and Frostick, 1984; Reid et al., 1985) studied the effects of inter-flood low flow on
37 subsequent sediment transport in Turkey Brook, England. They found that bedload transport rates were reduced during
38 relatively isolated flood events (e.g., events separated by long time intervals) compared to those that were closely spaced, with
39 the entrainment threshold up to as large as three times higher. They linked this with sediment reorganization during prolonged
40 periods of antecedent flow, which can make the river bed more armored and more resistant to entrainment, thus delaying the
41 onset of sediment mobility in the following flood event. Carling et al. (1992) also reported differences in the initial motion
42 criteria between flood events due to changes in the packing and orientation of sediment particles.

43 To further study such “memory” effects of antecedent flow on the sediment transport during a subsequent flood, a
44 number of flume experiments as well as field surveys have been conducted in the past decade, and different terms have been
45 proposed, including “stress history effect” (Monteith and Pender, 2005; Paphitis and Collins, 2005; Haynes and Pender, 2007;
46 Ockelford and Haynes, 2013), “flood history effect” (Mao, 2018), “flow history” (Masteller et al., 2019), ~~etc.~~ The difference
47 in the terminology could be partly due to the available data and the chosen approach in different research works. Given that
48 all these terms are similar, here we adopt the term “stress history” in this paper. It should also be noted that the approach
49 based on shear stress (and therefore terminology), even though widely applied for laboratory experiments, is much less reliable
50 for field measurements.

51 Paphitis and Collins (2005) conducted flume experiments to study the entrainment threshold of uniform sediment
52 subjected to antecedent flow durations of up to 120 minutes. They found that with a longer and higher antecedent flow, the
53 critical bed shear stress increases and the total bedload flux decreases. The work of Paphitis and Collins (2005) was extended
54 by Monteith and Pender (2005) and Haynes and Pender (2007) to consider bimodal sand-gravel mixtures. They found that for
55 a graded bed, longer periods of antecedent flow increase bed stability due to local particle rearrangement, in agreement with
56 Paphitis and Collins (2005); whereas higher magnitudes of antecedent flow reduce bed stability due to selective entrainment
57 of the fine matrix on bed surface, counter to Paphitis and Collins’ (2005) conclusion based on uniform sediment. Haynes and
58 Pender (2007) further analyzed the two competing effects and concluded that particle rearrangement may be of greater relative
59 importance than the winnowing of the fine sediment as it affects subsequent sediment transport. By using high resolution laser
60 scanning and statistical analysis of the bed topography, Ockelford and Haynes (2013) also demonstrated that the response of
61 bed topography to stress history is grade specific: bed roughness decreased in uniform beds but increased in graded bed with
62 an increase length of an antecedent flow period. Performing a series of flume experiments, Masteller and Finnegan (2017)
63 studied the evolution of the river bed on particle scale during low flow. They linked reduction of bedload flux to the re-
64 organization of the highest protruding grains (1%-5% of the entire bed) on bed surface.

65 Because of the above-mentioned research, existing sediment transport formulae for gravel-bed rivers (e.g. Meyer-
66 Peter and Müller, 1948; Parker, 1990; Wilcock and Crowe, 2003; Wong and Parker, 2006) are regarded to be inaccurate
67 because they do not take the effect of stress history into account. To this end, Paphitis and Collins (2005) proposed an empirical
68 formula for the exposure correction factor in the critical shear velocity for a uniform sand-size bed based on their experimental
69 data. Johnson (2016) developed a state function for the critical shear stress in terms of transport disequilibrium, which
70 incorporates the effects of stress history and hydrograph variability. Ockelford et al. (2019) proposed two forms of functions
71 to link the antecedent duration and the critical shear stress. The two alternatives proposed by Ockelford et al. (2019) correct
72 the function proposed by Paphitis and Collins (2005), whose exposure correction uses a logarithmic function which implicitly
73 assumes an unbound growth as antecedent time tends towards infinity.

74 Research to date has shown that antecedent flow can stabilize the river bed, thus influencing the threshold of sediment
75 motion as well as bedload flux. However, most of the previous research about stress history is either under conditions with
76 relatively low sediment transport or with relatively short durations of sediment transport in order to capture the threshold of
77 sediment motion (Monteith and Pender, 2005; Paphitis and Collins, 2005; Haynes and Pender, 2007; Ockelford and Haynes,
78 2013; Masteller and Finnegan, 2017; Ockelford et al., 2019). On the other hand, other researchers have found that exceptionally
79 high discharge events can reduce critical shear stress by disrupting particle interlocking and breaking of bed structure ([Lenzi,
80 2001; Turowski et al., 2009;](#) Turowski et al., 2011; Yager et al., 2012; Ferrer-Boix and Hassan 2015; Masteller et al., 2019).
81 Flume experiments by Masteller and Finnegan (2017) also indicate an increase in the number of highly mobile, highly
82 protruding grains in response to sediment transporting flows. Therefore, the effect of high discharge events in reducing the
83 critical shear stress likely counterbalances the stress history effect of antecedent flow to increase the critical shear stress.
84 [Besides, the supply of fine sediment \(during high discharge events\) is also widely observed to enhance the mobilization of
85 coarse sediment \(Wilcock et al., 2001; Curran and Wilcock, 2005; Venditti et al., 2010\).](#) In consideration of these opposing
86 mechanisms, how long can the stress history effect last during a subsequent flood event is not well understood. Such a question
87 is important especially in light of the fact that most sediment transport and channel adjustment of mountain gravel-bed rivers
88 occurs during high discharge events, when the flow shear stress is high.

89 In this paper, flume experiments consisting of ~~extended cycles of~~ high and low flow [areis](#) conducted to study this
90 problem. The experimental arrangement is described in Sect. 2. In Sect. 3, we present the experimental results showing how
91 channel morphology and sediment transport during a subsequent hydrograph respond to various durations of antecedent
92 conditioning flow. The threshold of motion is analyzed in Sect. 4 based on the experimental data. Implications and limitations
93 of this study are also discussed in Sect. 4. Finally, conclusions are summarized in Sect. 5.

94 **2 Experimental arrangements**

95 The experimental arrangements were guided by conditions observed in East Creek, a small mountain creek in Malcom
96 Knob Forest, University of British Columbia (for details on the study site see Papangelakis and Hassan, 2016). To investigate

97 the study objectives, we conducted flume experiments in the Mountain Channel Hydraulic Experimental Laboratory at the
98 University of British Columbia. The experiments were conducted in a tilting flume with a length of 5 m, a width of 0.55 m
99 and a depth of 0.80 m. The initial slope was 0.04 m/m. Water, but not sediment was recirculated by an axial pump. A set of
100 six experiments (REF2 – REF7) was conducted; the experimental conditions are briefly summarized in Table 1. For
101 experiments REF3 – REF7, the same hydrograph and sedimentograph were conducted, but with different durations of constant
102 conditioning flow prior to the hydrograph/sedimentograph. It should be noted that in the experiments, we only implemented
103 the rising limb of the hydrograph/sedimentograph, rather than a full hydrograph/sedimentograph with both rising and falling
104 limbs. Rather than studying river adjustment during a flow hydrographs, we aimed at determining the influence of conditioning
105 time on ~~the~~ bedload and bed surface arrangements as flow rates increased. We denote these as REF3 (10), REF4 (2), REF5 (5),
106 REF6 (15) and REF7 (0.25), with the numbers in the brackets denoting the duration of the conditioning flow in hours.
107 Experiment REF2 (15) consists of a 15-hour conditioning period without a subsequent hydrograph/sedimentograph, to test the
108 reproducibility of our experimental results during the conditioning flow.

109 **Table 1.** Summary of the experimental conditions and measurements. The experiments are listed in the table in order of decreasing duration of conditioning flow.

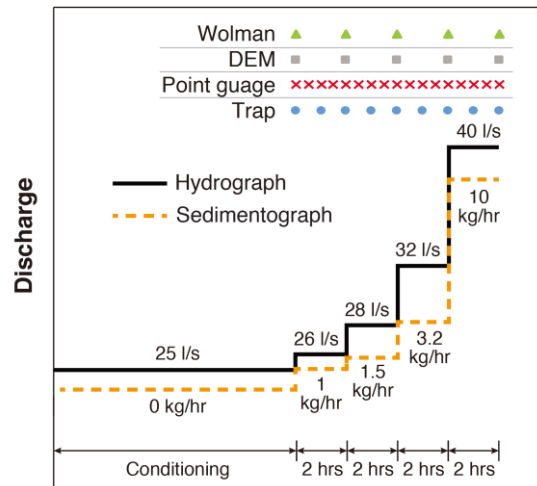
| No. | Phase | Duration (h) | Flow discharge (l/s) | Water surface slope (%) | Flow depth (cm) | Froude number (-) | τ_b (Pa) | Δz_b (mm) | Sediment feed (kg/h) | D_{s50} (mm) | D_{s90} (mm) | D_{150} (mm) | D_{190} (mm) | τ_{s50}^* | Q_s (kg/h) |
|-----------|--------------|--------------|----------------------|-------------------------|-----------------|-------------------|---------------|-------------------|----------------------|-------------------------------|-------------------------------|----------------|----------------|-------------------------------|--------------|
| REF2 (15) | Conditioning | 15 | 25 | 2.62 | 6.33 | 0.91 | 16.27 | <u>-30.2</u> | 0 | 15.2 <u>15.5</u> | 29.6 <u>29.7</u> | 1.07 | 5.43 | 0.069 <u>0.065</u> | 0.27 |
| REF6 (15) | Conditioning | 15 | 25 | 3.27 | 6.47 | 0.88 | 20.76 | <u>-16.6</u> | 0 | 15.87 <u>15.7</u> | 30.69 <u>30.8</u> | 35.18 | 42.84 | 0.089 <u>0.082</u> | 0.89 |
| | Step 1 | 2 | 26 | 3.34 | 6.39 | 0.94 | 20.93 | <u>0.3</u> | 1 | 15.66 <u>15.44</u> | 29.98 <u>29.0</u> | 12.51 | 39.38 | 0.083 <u>0.090</u> | 0.68 |
| | Step 2 | 2 | 28 | 3.10 | 6.29 | 1.03 | 19.13 | <u>0.0</u> | 1.5 | 17.18 <u>17.3</u> | 30.40 <u>30.94</u> | 7.28 | 27.59 | 0.069 <u>0.068</u> | 0.76 |
| | Step 3 | 2 | 32 | 3.06 | 6.80 | 1.05 | 20.41 | <u>-1.9</u> | 3.2 | 15.34 <u>15.62</u> | 30.85 <u>30.18</u> | 12.39 | 36.54 | 0.082 <u>0.078</u> | 6.73 |
| | Step 4 | 2 | 40 | 2.81 | 7.78 | 1.07 | 21.45 | <u>-16.1</u> | 10 | 15.95 <u>15.9</u> | 30.34 <u>30.16</u> | 11.48 | 36.03 | 0.083 <u>0.083</u> | 13.39 |
| REF3 (10) | Conditioning | 10 | 25 | 2.73 | 6.02 | 0.98 | 16.12 | <u>-25.8</u> | 0 | 14.91 <u>14.8</u> | 29.52 <u>29.2</u> | 2.17 | 9.98 | 0.071 <u>0.067</u> | 0.28 |
| | Step 1 | 2 | 26 | 2.75 | 5.93 | 1.04 | 16.00 | <u>0.1</u> | 1 | 15.01 <u>15.6</u> | 29.32 <u>29.5</u> | 2.55 | 19.94 | 0.066 <u>0.063</u> | 1.71 |
| | Step 2 | 2 | 28 | 2.69 | 6.35 | 1.01 | 16.77 | <u>0.3</u> | 1.5 | 15.51 <u>15.8</u> | 29.73 <u>29.2</u> | 4.06 | 26.99 | 0.067 <u>0.065</u> | 2.19 |
| | Step 3 | 2 | 32 | 2.88 | 6.81 | 1.04 | 19.25 | <u>-1.7</u> | 3.2 | 15.91 <u>15.9</u> | 29.73 <u>29.1</u> | 6.18 | 24.26 | 0.075 <u>0.075</u> | 2.44 |
| | Step 4 | 2 | 40 | 2.48 | 8.34 | 0.96 | 20.28 | <u>-8.0</u> | 10 | 15.61 <u>15.2</u> | 32.83 <u>32.8</u> | 14.45 | 39.13 | 0.080 <u>0.088</u> | 12.45 |
| REF5 (5) | Conditioning | 5 | 25 | 3.26 | 5.51 | 1.12 | 17.63 | <u>-16.8</u> | 0 | 16.35 <u>16.53</u> | 31.14 <u>31.2</u> | 8.23 | 25.34 | 0.066 <u>0.071</u> | 0.49 |
| | Step 1 | 2 | 26 | 3.24 | 6.19 | 0.98 | 19.68 | <u>-0.6</u> | 1 | 16.30 <u>16.54</u> | 30.90 <u>31.5</u> | 6.57 | 23.63 | 0.075 <u>0.079</u> | 2.24 |
| | Step 2 | 2 | 28 | 3.09 | 6.21 | 1.05 | 18.82 | <u>-0.3</u> | 1.5 | 16.87 <u>17.2</u> | 31.27 <u>31.4</u> | 9.38 | 28.44 | 0.069 <u>0.067</u> | 3.30 |
| | Step 3 | 2 | 32 | 3.05 | 6.65 | 1.08 | 19.91 | <u>-1.2</u> | 3.2 | 16.04 <u>16.8</u> | 31.04 <u>31.9</u> | 11.90 | 47.91 | 0.077 <u>0.073</u> | 5.72 |
| | Step 4 | 2 | 40 | 2.78 | 7.82 | 1.06 | 21.33 | <u>-13.4</u> | 10 | 14.72 <u>15.1</u> | 31.44 <u>31.45</u> | 15.09 | 38.56 | 0.090 <u>0.087</u> | 40.03 |

| | | | | | | | | | | | | | | | |
|----------------|--------------|------|----|------|------|------|-------|--------------|-----|---------------------------------|---------------------------------|-------|-------|----------------------------------|-------|
| REF4 (2) | Conditioning | 2 | 25 | 2.82 | 5.55 | 1.11 | 15.34 | <u>-17.8</u> | 0 | 13.581 <u>2.3</u> | 28.782 <u>7.8</u> | 3.10 | 15.79 | 0.0700.0 <u>77</u> | 1.50 |
| | Step 1 | 2 | 26 | 2.73 | 5.55 | 1.16 | 14.85 | <u>-0.5</u> | 1 | 14.641 <u>4.8</u> | 28.832 <u>8.9</u> | 3.90 | 20.31 | 0.0630.0 <u>62</u> | 0.96 |
| | Step 2 | 2 | 28 | 2.71 | 6.19 | 1.06 | 16.46 | <u>-0.1</u> | 1.5 | 15.441 <u>5.6</u> | 29.092 <u>9.2</u> | 6.28 | 46.76 | 0.0660.0 <u>65</u> | 2.41 |
| | Step 3 | 2 | 32 | 3.15 | 6.85 | 1.04 | 21.15 | <u>-6.4</u> | 3.2 | 14.441 <u>4.5</u> | 28.652 <u>8.8</u> | 17.34 | 37.76 | 0.0910.0 <u>90</u> | 26.73 |
| | Step 4 | 2 | 40 | 2.76 | 8.01 | 1.02 | 21.69 | <u>-7.7</u> | 10 | 14.061 <u>3.7</u> | 30.222 <u>9.7</u> | 10.88 | 35.45 | 0.0950.0 <u>98</u> | 5.23 |
| REF7 (0.25) | Conditioning | 0.25 | 25 | 3.46 | 6.20 | 0.94 | 21.06 | <u>-14.9</u> | 0 | 14.671 <u>4.0</u> | 30.102 <u>9.5</u> | 10.54 | 28.03 | 0.0890.0 <u>93</u> | 19.44 |
| | Step 1 | 2 | 26 | 3.20 | 6.54 | 0.90 | 20.53 | <u>-4.8</u> | 1 | 15.521 <u>5.6</u> | 30.863 <u>1.6</u> | 7.11 | 28.91 | 0.0820.0 <u>81</u> | 3.48 |
| | Step 2 | 2 | 28 | 3.14 | 6.58 | 0.96 | 20.27 | <u>-0.7</u> | 1.5 | 16.621 <u>6.2</u> | 31.332 <u>1.2</u> | 6.91 | 30.73 | 0.0750.0 <u>77</u> | 2.52 |
| | Step 3 | 2 | 32 | 3.12 | 7.00 | 1.00 | 21.41 | <u>-4.5</u> | 3.2 | 14.891 <u>4.3</u> | 30.783 <u>0.5</u> | 10.09 | 37.40 | 0.0890.0 <u>92</u> | 12.32 |
| | Step 4 | 2 | 40 | 2.73 | 8.29 | 0.97 | 22.19 | <u>-9.6</u> | 10 | 17.681 <u>7.3</u> | 36.203 <u>3.6</u> | 12.13 | 30.78 | 0.0780.0 <u>79</u> | 16.80 |

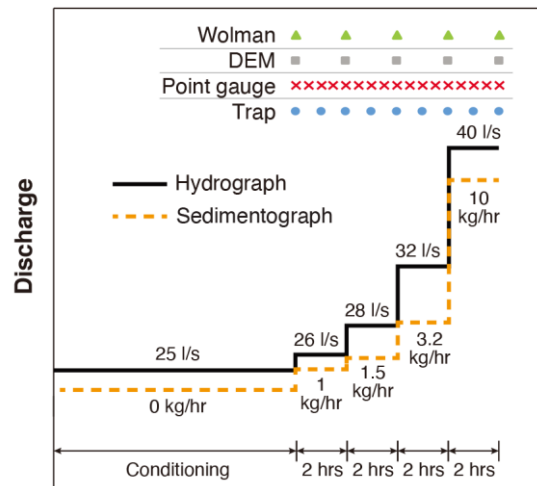
110 a. Q_s : bedload transport rate, Δz_b : mean difference of bed elevation averaged over the whole river channel, τ_b : shear stress, D_{s50} and D_{s90} : D_{50} and D_{90} of bed surface,
111 D_{l50} and D_{l90} : D_{50} and D_{90} of bedload, τ_{s50}^* : Shields number for D_{s50} . Here D_{90} denotes the grain size such that 90% is finer, and D_{50} denotes the grain size such that
112 50% is finer. All values presented in this table are measured at the end of each stage, except for Δz_b , which denotes the mean difference of bed elevation during
113 each stage (i.e., difference between the end of this stage and the end of last stage). A positive value of Δz_b denotes aggradation, and a negative value of Δz_b denotes
114 degradation.

115

116 Figure 1 shows the water and sediment supply implemented ~~during~~ the experiments. The water discharge
 117 was selected to represent typical flows in East Creek, with the 25 l/s flow during the conditioning period being
 118 equivalent to half the bankfull flow, and the peak flow discharge of 40 l/s during the hydrograph being about 1.1 times
 119 the bankfull flow in East Creek. Because the purpose of this paper is to study the evolution of bed stability, sediment
 120 was not fed during the conditioning flow. For each step of the hydrograph, the feed rate of sediment was specified to
 121 be close to the transport capacity of the flow. Determination of the sediment supply rates was facilitated by a numerical
 122 model which ~~was had been~~ calibrated ~~for with~~ similar experimental conditions (Ferrer-Boix and Hassan, 2014).we
 123 chose a feed rate through numerical simulations following Ferrer Boix and Hassan (2014) in combination with trial
 124 experiments. Sediment was fed into the flume at the upstream end using a conveyor belt feeder at the calculated
 125 transport rate capacity. The feed rate of the sedimentograph ranged between 1 kg/hour and 10 kg/hour. Both
 126 the hydrograph and the sedimentograph consisted of four steps, with each step lasting for 2 hours.



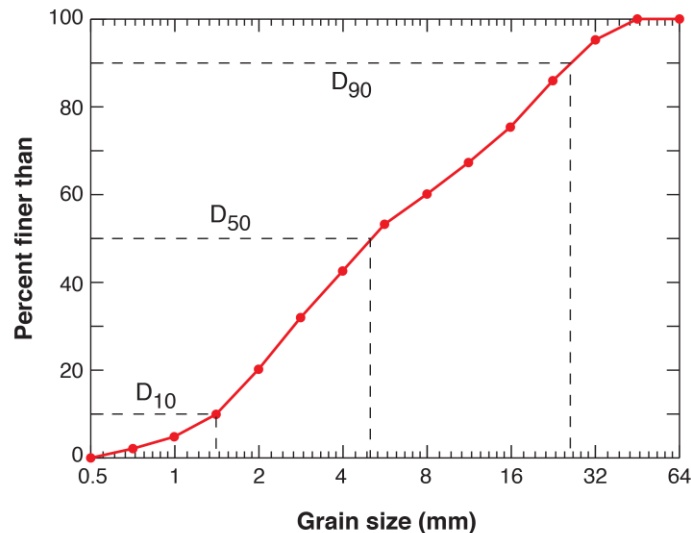
127



128

129 **Figure 1.** Water and sediment supply implemented in the experiments. Markers in top of the figure denote the time
130 of measurements during the hydrograph phase. Time of measurements during the conditioning phase is not shown in
131 this figure.

132 Figure 2 shows the GSD of the bulk sediment used in the experiments, with the grain size ranging between
133 0.5 and 64 mm. The GSD was scaled from East Creek by a ratio of 1:4, except that sediment (after scaling) with a
134 grain size less than 0.5 mm was excluded. This preserved the entire gravel distribution of East Creek with a maximum
135 size of 256 mm (scaled to 64 mm in Fig. 2). The model was “generic” rather than specific. This means -in that no
136 attempt was made to reproduce the geometric details of the prototype channel. The bulk sediment was sieved at half
137 ϕ intervals and each grain size class was painted in different colors for each size class for texture analysis and visual
138 identification. Before the commencement of each experiment, we hand-mixed and screeded-leveled the bulk sediment
139 to make a flat and uniform layer of loose material with a depth of 0.15 m. The sediment was then slowly flooded and
140 then drained to aid settlement. The bulk sediment was also used for the sediment feed in each experiment.



141 **Figure 2.** Grain size distribution of the bulk sediment used in the experiments.
142

143 The elevations of the bed surface and water surface elevations were measured along the flume every 0.25 m
144 using a mechanical point gauge with a precision of ± 0.001 m. Water depth fluctuations due to wave effects at a point
145 were about 5% or less. Water surface slope and bed slope are calculated based on a linear regression of the point gauge
146 data measured between 0.5 m and 4.75 m upstream of the outlet. The most upstream and downstream sections are
147 excluded to avoid boundary effects. A green laser scanner mounted on a motorized cart was also used to measure the
148 bed surface elevation along the flume. Bed laser scans were composed of cross sections spaced 2 mm apart with 1 mm
149 vertical and horizontal accuracy (for details see Elgueta-Astaburuaga and Hassan, 2017). The standard deviation of
150 bed elevation was calculated based on the DEM data from scans. Before the calculation of standard deviation, the
151 DEM was detrended based on linear regression to remove spatial trends with scales larger than the scale of sediment
152 patterns (e.g., bed slope or undulations). To estimate the particle size distribution of the bed surface we used digital
153 cameras mounted on a motorized cart along the entire flume. Images were merged together to visualize the bed and

154 ~~perform~~ perform the particle size analysis (Chartrand et al., 2018). To avoid the distortion effects due to image merging,
155 the width of the image strips that were stitched to get a composite image was specified as just 2 cm. The particle size
156 distribution of the bed surface was estimated using the Wolman (point count) method, by identifying the grain size of
157 particles at the intersections of a 5 cm grid superimposed on the photograph.~~The particle size distribution of the bed~~
158 ~~surface was estimated using the grid by number (point counts) method, by identifying particle size at the intersection~~
159 ~~of a 5 cm grid superimposed on each photograph.~~ Individual grains were identified by color. ~~Collected data~~For each
160 experiment, the grain size distribution of the bed surface was calculated at different times to quantify its changes
161 during the experiment. ~~were used to quantify changes in the bed surface particle size distribution throughout each~~
162 ~~experiment.~~

163 ~~Material evacuated from the flume was trapped in a 0.25 mm mesh screen in the tailbox, and weighted and~~
164 ~~sieved at half ϕ intervals to calibrate a light table.~~ The sediment transport rates for various size ranges were measured
165 at the end of the flume using a light table (for details see Zimmerman et al., 2008; Elgueta-Astaburuaga and Hassan
166 2017) and automated image analysis at a resolution of 1 second (for details see Zimmerman et al., 2008; Elgueta-
167 Astaburuaga and Hassan 2017). ~~Material evacuated from the flume was also trapped in a 0.25 mm mesh screen in the~~
168 ~~tailbox, and weighted and sieved at half ϕ intervals, and then used to calibrate the light table data.~~ To avoid random
169 fluctuations in sediment transport, we report the bedload transport rate measured by light table at a 5-minute resolution,
170 and characteristic grain sizes of bedload at 15-minute resolution. A range of methods for the estimation of bed shear
171 stress has been suggested in the literature (reviewed in Whiting and Dietrich, 1990). In this study, the shear stress is
172 estimated using the depth-slope product corresponding to normal (steady and uniform) flow. This method is selected
173 because the focus of this work is on overall (mean) parameters controlling bed evolution; in addition, the water was
174 too shallow to use an ADV. The water surface slope, rather than bed slope, is implemented in the calculation of shear
175 stress, with the consideration that water surface slope is closer to the friction slope and also has less random
176 fluctuations than bed slope.

177 The frequency of measurements during the hydrograph phase is also plotted in Fig. 1(a), with the point gauge
178 measurements conducted every 30 minutes, the trap weighting/sampling conducted every hour, and the DEM/Wolman
179 measurements by laser scan/photograph conducted every 2 hours (i.e. at the beginning/end of each stage of the
180 hydrograph). For each measurement of DEM/Wolman, we stopped the pump instantaneously and let the flow ~~was~~
181 ~~slowly lowered~~ and then ~~stopped~~ to allow for the bed to be scanned by a laser and photographed. The time interval
182 between the stop of the pump and the stop of the flow was about 3 to 4 minutes. To avoid the influence of the following
183 rising discharge, all subsequent measurements were taken after the flow became stable. The frequency of measurement
184 during the conditioning phase was adjusted in each experiment in accordance with the duration of the conditioning
185 phase, and is therefore not plotted in Fig. 1(a).

186 The uncertainties of associated with the measurement are also studied. For the uncertainties of the standard
187 deviation of bed elevation, we scanned the floor of the flume twice and calculated the standard deviations of the
188 scanned DEM. The floor of the flume was horizontal and flat, with no sediment on the bed. Theoretically, the standard
189 deviation of the DEM should be zero. Therefore, the calculated standard deviations of the flume floor are regarded as
190 an estimation of the uncertainties of our calculations during experiment. To estimate the uncertainties of the bed

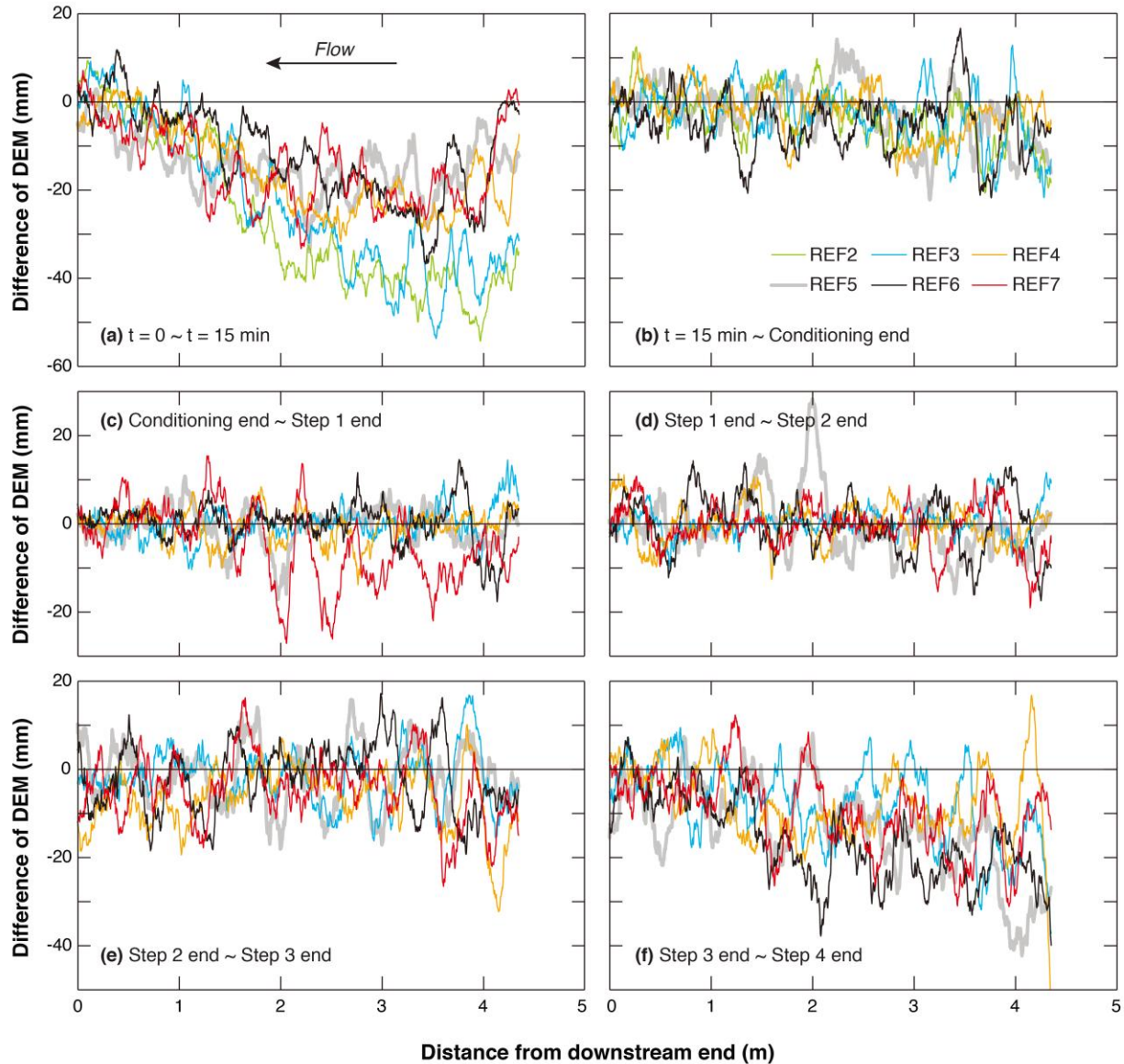
191 surface GSD, for each measurement the Wolman method was implemented for 5 times on the same photograph, with
192 100 samples/counts for each time. The 5 measured GSDs for each time interval were used to calculate the mean and
193 standard deviation of the bed surface texture (in terms of D_{s10} , D_{s50} , and D_{s90}). To estimate the uncertainties of the light
194 table method, we compare the data measured by the light table with the data measured by the sediment trap, in terms
195 of both sediment transport rate and the characteristic grain sizes of sediment load. To estimate the variations of the
196 measured/calculated data, we calculate their coefficient of variation (cv), which is defined as the ratio of the standard
197 deviation to the mean value.

198 3 Experimental results

199 Table 1 presents an overall schematization of the experimental results, including water surface slope, flow
200 depth h , Froude number F_r ($F_r = u / (gh)^{0.5}$), where u is depth-averaged flow velocity), bedload transport rate Q_s , shear
201 stress τ_b , D_{50} and D_{90} of bed surface (D_{s50} and D_{s90}), D_{50} and D_{90} of bedload (D_{l50} and D_{l90}), and Shields number τ_{s50}^*
202 for a given D_{s50} . Here D_{90} denotes the grain size such that 90% is finer, and D_{50} denotes the grain size such that 50%
203 is finer.

204 3.1 Channel adjustment

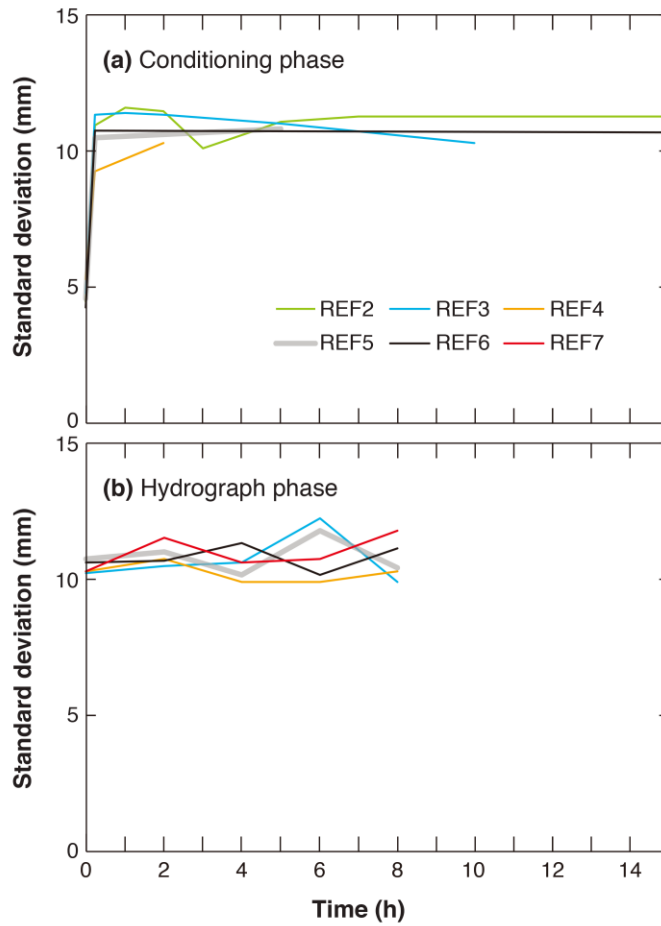
205 In this section, we present the channel adjustments during each experiment. Figure 3 shows the difference of
206 longitudinal DEM averaged over the cross section, which can represent the adjustment of channel topography during
207 different periods of the experiment. The DEM averaged over the cross section is used here to study the overall
208 aggradation/degradation of the channel. For reference, detailed information about the DEM at different times during
209 the experiment is provided in the Supporting Information, with REF6 (15) as an example. From Fig. 3(a) we can see
210 that for each experiment, evident degradation occurs during the first 15 minutes, especially at the upstream end of the
211 flume. This is due to the fact that no sediment supply is implemented during the conditioning period, and also the
212 initial bed material is relatively loose. From 15 minutes until the end of the conditioning phase (as shown in Fig. 3(b)),
213 no evident aggradation/degradation is observed for any experiment, indicating that most of the adjustment of channel
214 topography during the conditioning phase has been accomplished within the first 15 minutes. For Step 1 of the
215 hydrograph (as shown in Fig. 3(c)), no evident aggradation/degradation is observed for any of the experiments (with
216 the mean difference of bed elevation Δz_b less than ± 1 mm, as shown in Table 1), except for REF7 (0.25), which has
217 the shortest conditioning phase and experienced a mean degradation of 4.8 mm over the whole bed channel. Similarly,
218 the channel keeps relatively stable during Step 2 of the hydrograph for all experiments (as shown in Fig. 3(d)), with
219 no evident trend for aggradation/degradation being observed (the mean difference of bed elevation Δz_b is less than ± 1
220 mm for all experiments). With the increase of flow discharge, some degradation (with a magnitude of about 10 ~ 20
221 mm) can be observed in Step 3 for all experiments at the upstream end of the channel, as shown in Fig. 3(e). Such
222 degradation becomes more evident over the entire channel in Step 4 of the hydrograph, when flow discharge reaches
223 its peak value. This is in agreement with the values of Δz_b presented in Table 1. Further analysis of the DEM data
224 shows that no bedform were evident during the experiment.



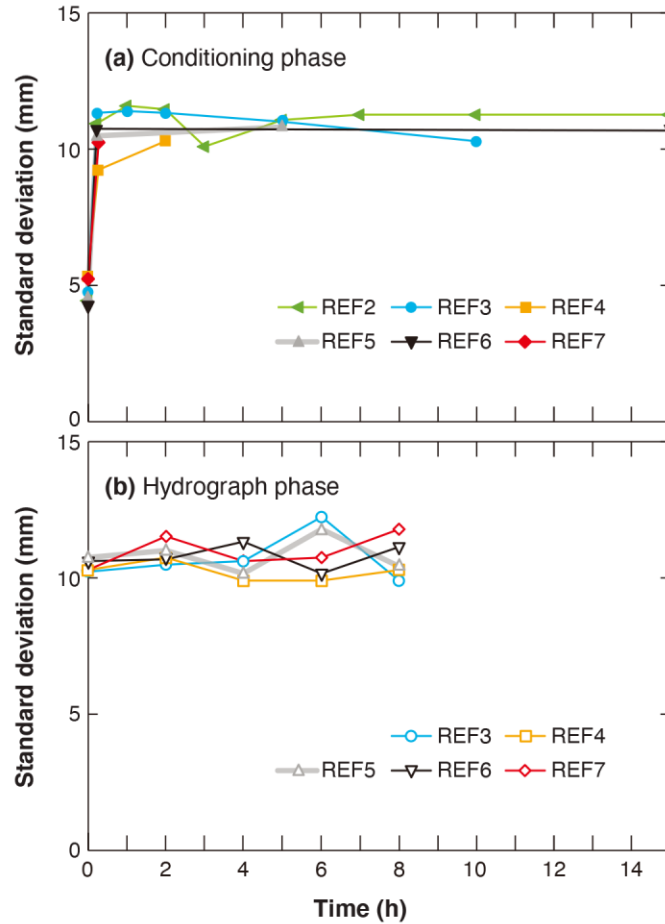
225
 226 **Figure 3.** Spatial distribution of elevation difference from cross-sectionally averaged longitudinal DEM during the
 227 experiment: (a) from beginning of experiment to $t = 15$ minutes; (b) from $t = 15$ minutes to the end of conditioning
 228 phase; (c) from the end of conditioning phase to the end of Step 1 of hydrograph phase; (d) from the end of Step 1 to
 229 the end of Step 2 of the hydrograph phase; (e) from the end of Step 2 to the end of Step 3 of the hydrograph phase; (f)
 230 from the end of Step 3 to the end of Step 4 of the hydrograph phase.

231 Figure 4 shows the temporal variation of the standard deviation of bed elevation, which is often scaled with
 232 the bed roughness for gravel-bed rivers (see Chen et al. (2020) for a detailed discussion on this topic), over the length
 233 of the erodible bed during the experiment. Results show that the standard deviation of bed elevation is relatively small
 234 at the beginning of the experiments (corresponding to a relatively smooth bed depending on the way we prepared the
 235 initial bed), but increases notably within 15 minutes after the start of the conditioning phase. Such an increase of the
 236 bed roughness standard deviation of bed elevation is accompanied by significant degradation during the first 15

237 minutes, as shown in Fig. 3(a). The standard deviation of bed elevation ~~remains almost constant~~ becomes quite stable
 238 during the remaining conditioning phase, as well as during the hydrograph phase, despite the fact that degradation is
 239 evident as the flow approaches its peak value. For the standard deviation of bed elevation during the conditioning
 240 phase, we calculate the coefficient of variation (cv) for REF2 (15), which has the longest conditioning phase. T, and
 241 the result shows a value of 0.038 from $t = 15$ minutes to the end of conditioning flow. For the standard deviation of
 242 bed elevation during the hydrograph phase, we calculate the cv for all experiments; and the results shows that the
 243 values of cv vary between 0.031 and 0.075. Besides, the value of standard deviation is almost identical for each
 244 experiment, indicating the period of conditioning phase exerts little effect on the standard deviation of bed elevation.



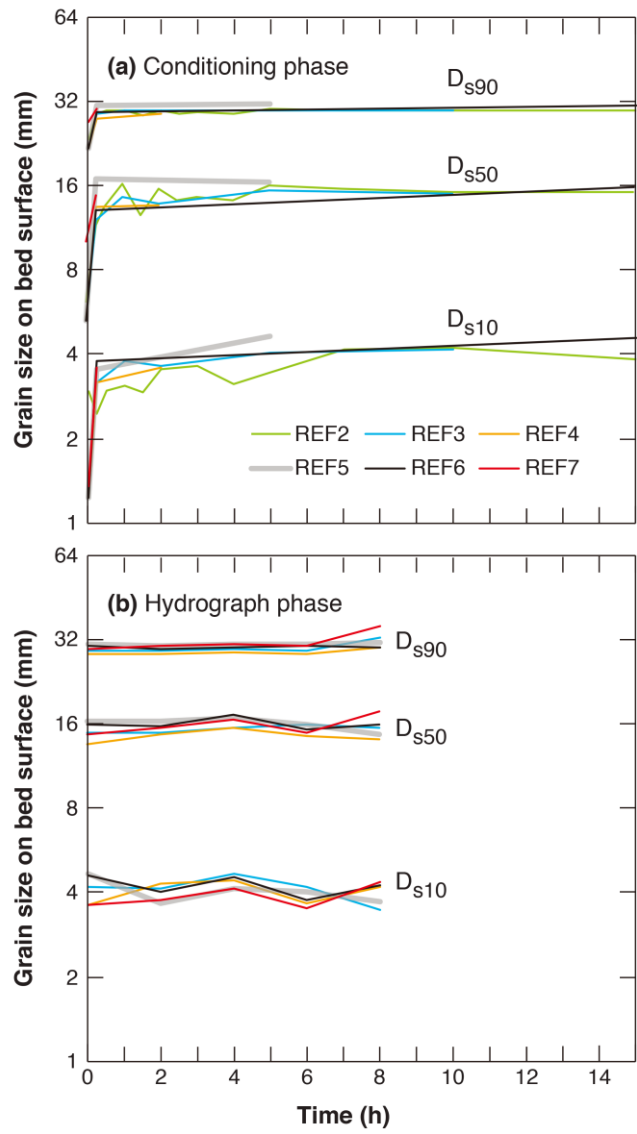
245



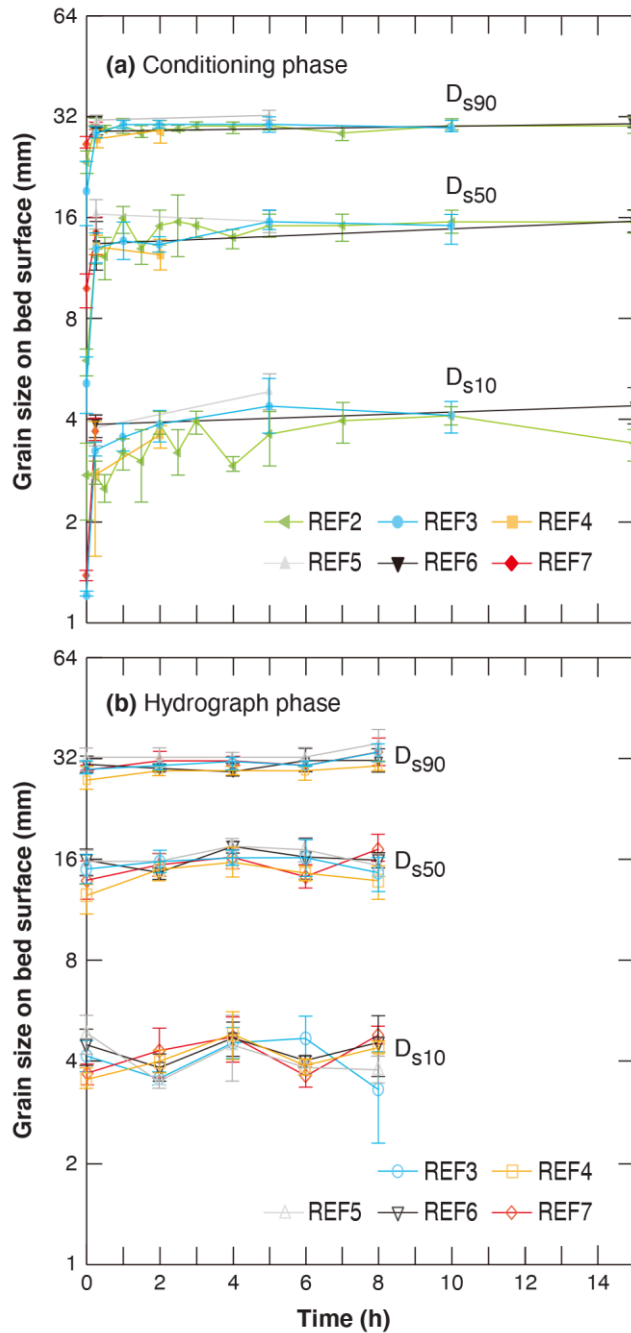
246
 247 **Figure 4.** Temporal adjustments of standard deviation of bed elevation calculated over the whole erodible bed: (a) the
 248 conditioning phase; (b) the hydrograph phase. The uncertainties of the calculation is in the range of 1.6~2.5 mm,
 249 which is close to the vertical resolution of the laser (1 mm).

250 Figure 5 shows the temporal variation of the characteristic grain size of bed surface material, as well as an
 251 estimation of the uncertainties of associated with measurements of the surface texture. Three parameters are
 252 presented here; D_{s10} , D_{s50} , and D_{s90} . The adjustment of bed surface GSD follows similar trends as the adjustment of
 253 standard deviation of bed elevation. That is, for all experiments, the bed surface is fine at the beginning, and
 254 experiences a fast coarsening period during the first 15 minutes (along with the bed degradation in Fig. 3 and the
 255 increase of bed roughness in Fig. 4). The characteristic grain sizes of bed surface remain relatively stable after the first
 256 15 minutes, despite variabilities due to the measurement uncertainty. For REF2 (15) which has the longest
 257 conditioning phase, cv (coefficient of variation) values of the mean D_{s10} , D_{s50} , and D_{s90} (over the five repeated
 258 measurements) are 0.15, 0.09, and 0.02 respectively from $t = 15$ minutes to the end of the conditioning flow. It is
 259 worth noted-noting that the GSD of bed surface keeps relatively constant even during the hydrograph phase, during
 260 which a flood event is introduced in the flume and evident bed degradation is observed. For each experiment, the cv
 261 values of the mean D_{s10} , D_{s50} , and D_{s90} (over the five repeated measurements) are less than 0.13, 0.08, and 0.04

262 respectively during the hydrograph phase. This is in agreement with the observation of Ferrer Boix and Hassan (2015)
263 during successive water pulses.



264



265

266

267

268

269

270

271

272

Figure 5. Temporal adjustments of characteristic grain sizes of bed surface material calculated over the whole erodible bed: (a) the conditioning phase; (b) the hydrograph phase. Markers show mean values of five repeated Wolman measurements. Range bars show the mean values \pm the standard deviations of the five repeated Wolman measurements.

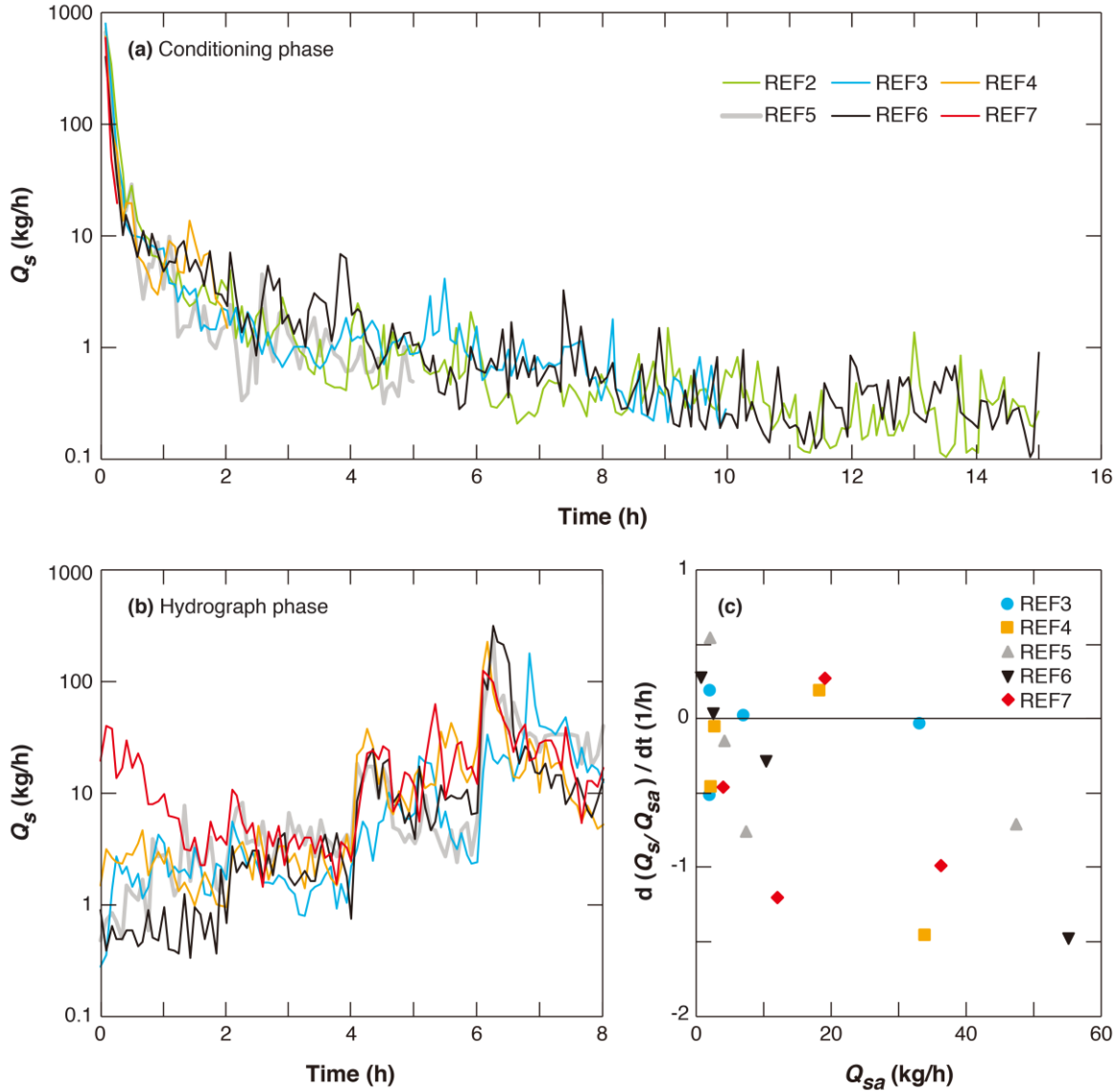
3.2 Sediment transport

In Fig. 6 we ~~exhibit~~present the instantaneous sediment transport rate Q_s , measured by the light table ~~in~~during each experiment. Sediment transport is reported every 5 minutes, as described in Sect. 2. Accuracy of the results is estimated by comparing the light table data with the data measured by the trap. Results show that for our experiments,

273 the light table method has good accuracy in terms of the sediment transport rate, with an overestimation by 4% on
274 average (111 samples and a standard deviation of 14.5%). 70 out of 111 samples show an accuracy of $\pm 10\%$, and 93
275 out of 111 samples show an accuracy of $\pm 20\%$. Details of this uncertainty analysis are presented in the Supporting
276 Information.

277 It can be seen in Fig. 6(a) that the temporal variation of sediment transport rate during the conditioning phase
278 follows the same trend in all six experiments. That is, the sediment transport rate decreases significantly during the
279 conditioning phase, with the decreasing rate being very large at the beginning and then gradually dropping. In the first
280 15 minutes, the sediment transport rates drop from more than 500 kg/hourkg/h to less than 100 kg/hourkg/h.
281 Afterwards, it takes about another 2 hours for the sediment transport rates to drop to close to 1 kg/hourkg/h. The
282 sediment transport rate eventually approaches a small and relatively constant value after about 8 hours of conditioning
283 flow. For REF2 (15) and REF6 (15) which have the longest conditioning phase, the sediment transport rates between
284 $t = 8$ hour and the end of conditioning phase ($t = 15$ hour) show mean values of 0.35 kg/hourkg/h (standard deviation
285 $= 0.22$ kg/h) and 0.37 kg/hourkg/h (standard deviation $= 0.24$ kg/h), respectively. Nevertheless, there are random high
286 points in the sediment transport rate even after 8 hours, despite no sediment feed from the inlet. These spikes imply
287 that partial destruction (or reorganization) of the bed structure occurs even after a long duration of conditioning.

288 Previous researchers (Haynes and Pender, 2007; Masteller and Finnegan, 2017) have suggested that an
289 exponential function can be implemented to describe such a decrease of sediment transport rate under conditioning
290 flow. Additional analysis is implemented in the Supporting Information to fit REF2 (15) and REF6 (15) (which have
291 the longest duration of conditioning phase) against a two-parameter exponential function. Results show that the
292 exponential function can describe the general decreasing trend of sediment transport rate during the conditioning phase,
293 except at the beginning of the experiment where the decrease of sediment transport rate is much more significant than
294 that predicted by the exponential function. Readers can refer to the Supporting Information for more details.



295 **Figure 6.** Instantaneous sediment transport rate measured by light table during (a) the conditioning phase; and (b) the
 296 hydrograph phase. (c) Intra-step temporal change rate of Q_s , normalized against Q_{sa} for each hydrograph step. Q_s is the
 297 sediment transport rate, and Q_{sa} is the averaged sediment transport rate of a given hydrograph step.
 298

299 Figure 6(b) presents the instantaneous sediment transport rate during the hydrograph phase. Results show
 300 that variation of sediment transport rate among different experiments prevails in the first step of the hydrograph, with
 301 the highest sediment transport rate for the experiment with the shortest conditioning duration (REF7 (0.25)); and the
 302 smallest sediment transport rate for the experiment with the longest conditioning duration (REF6 (15)). Such variation
 303 among experiments, however, diminishes towards the end of Step 1 and is not observed in the following three steps
 304 of the hydrograph, with the line for each experiment collapsing together in the figure. ~~The Such~~ adjustments of
 305 sediment transport rate are consistent with the process of channel deformation shown in Fig. 3-. That is, for both
 306 sediment transport and channel deformation, where the pattern of variation in results of REF7 (0.25) deviates from

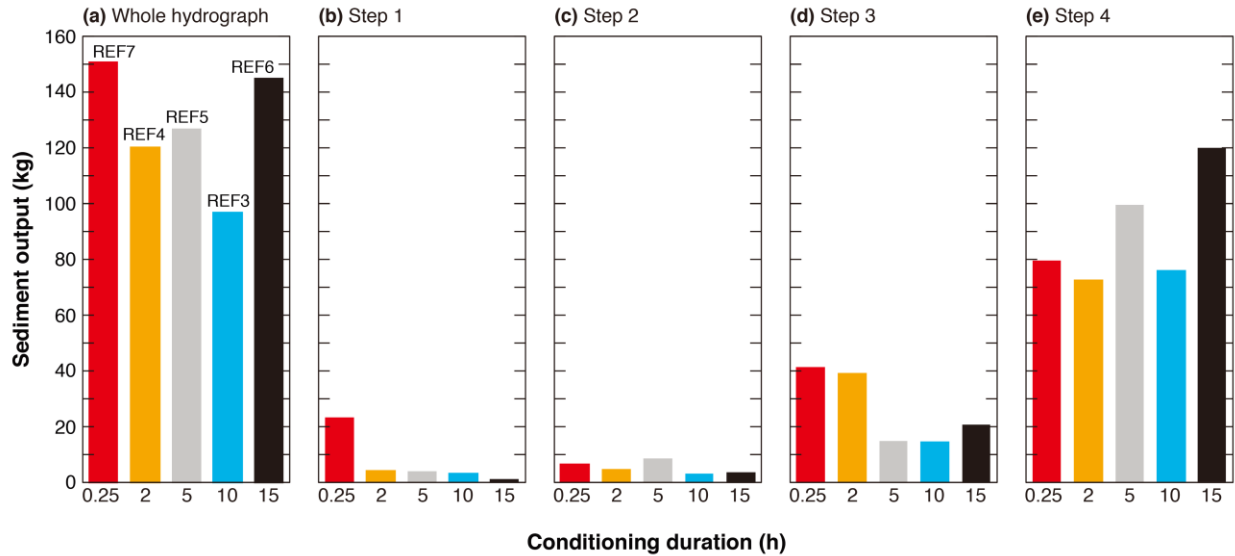
307 other experiments in Step 1 (larger sediment transport rate and more degradation in REF7 (0.25)), but collapses with
308 other experiments in the following three steps.

309 Results in Fig. 6(b) also show large variations of sediment transport rate during each step of the hydrograph.
310 Such intra-step variations of sediment transport rate are investigated in Fig. 6(c), with the x axis being the averaged
311 sediment transport rate of each step Q_{sa} and the y axis being $d(Q_s/Q_{sa})/dt$, ~~which~~ The value of $d(Q_s/Q_{sa})/dt$ is estimated
312 by linear regression. Here the instantaneous sediment transport rate Q_s is scaled against the average sediment transport
313 rate of the corresponding step Q_{sa} , in order to facilitate the comparison among different hydrograph steps.

314 Results in Fig. 6(c) shows that a large fraction of the data (11 out of 20) exhibits a decreasing trend in time
315 for Q_s (i.e. a negative value in vertical coordinate). Basically, the larger the averaged sediment transport rate Q_{sa} , the
316 larger ~~is~~ the rate of reduction in Q_s . Ferrer-Boix and Hassan (2015) observed similar declines in sediment transport
317 during their water pulses experiments. They attributed this to (1) the presence of bed structures, which could have
318 reduced skin friction up to 20% and (2) streamwise changes in the patterns of bed surface sorting. Out of 20 datasets,
319 5 exhibit some temporally increasing trend in Q_s (though not as evident as the decreasing trend mentioned before).
320 They are REF5 (5), REF3 (10), REF6 (15) during the first step; and REF7 (0.25), REF4 (2) during the third step. This
321 shows that for the three experiments with long conditioning duration, Q_s is very low at the end of the conditioning
322 phase, and the first step of the hydrograph sees a temporally increasing trend in Q_s . Whereas for the two experiment
323 with short conditioning phase, Q_s is still high at the end of the conditioning, so that the sediment transport rate keeps
324 decreasing during the first step, until in the third step an increasing trend in Q_s is observed, at which the water and
325 sediment supply become evidently higher. The decreasing/increasing trends of Q_s during steps of the hydrograph
326 reflect the transient adjustments of the bed to the changed water and sediment supply before equilibrium is achieved.

327 Sediment collected in the trap/tailbox at the flume outlet allows us to plot the total amount of sediment output
328 during each step of the hydrograph. To better understand the effect of the conditioning duration on sediment transport,
329 we calculate the cumulative sediment transport during the entire hydrograph phase as well as each step of the
330 hydrograph. Fig. 7(a) shows ~~that~~ the total sediment output during the entire hydrograph. It can be seen that the effect
331 of conditioning duration on the total sediment output during the entire hydrograph phase is not evident: a longer
332 duration of conditioning flow does not necessarily lead to a smaller (or larger) sediment output. The largest sediment
333 output occurs in REF7 (0.25), which is 55% larger than the sediment output in REF3 (10) which has the smallest
334 output, but is about the same as (only 4% larger than) the sediment output in REF6 (15). We further calculate the
335 correlation coefficient between the total sediment output and the duration of conditioning flow, and obtain a value of
336 $r = -0.14$, indicating that there is almost no correlation between the two parameters. ~~does not show much differencee~~
337 ~~for each experiment, indicating that the duration of conditioning flow does not pose much influence on the total volume~~
338 ~~of sediment transport during the subsequent flood.~~

339



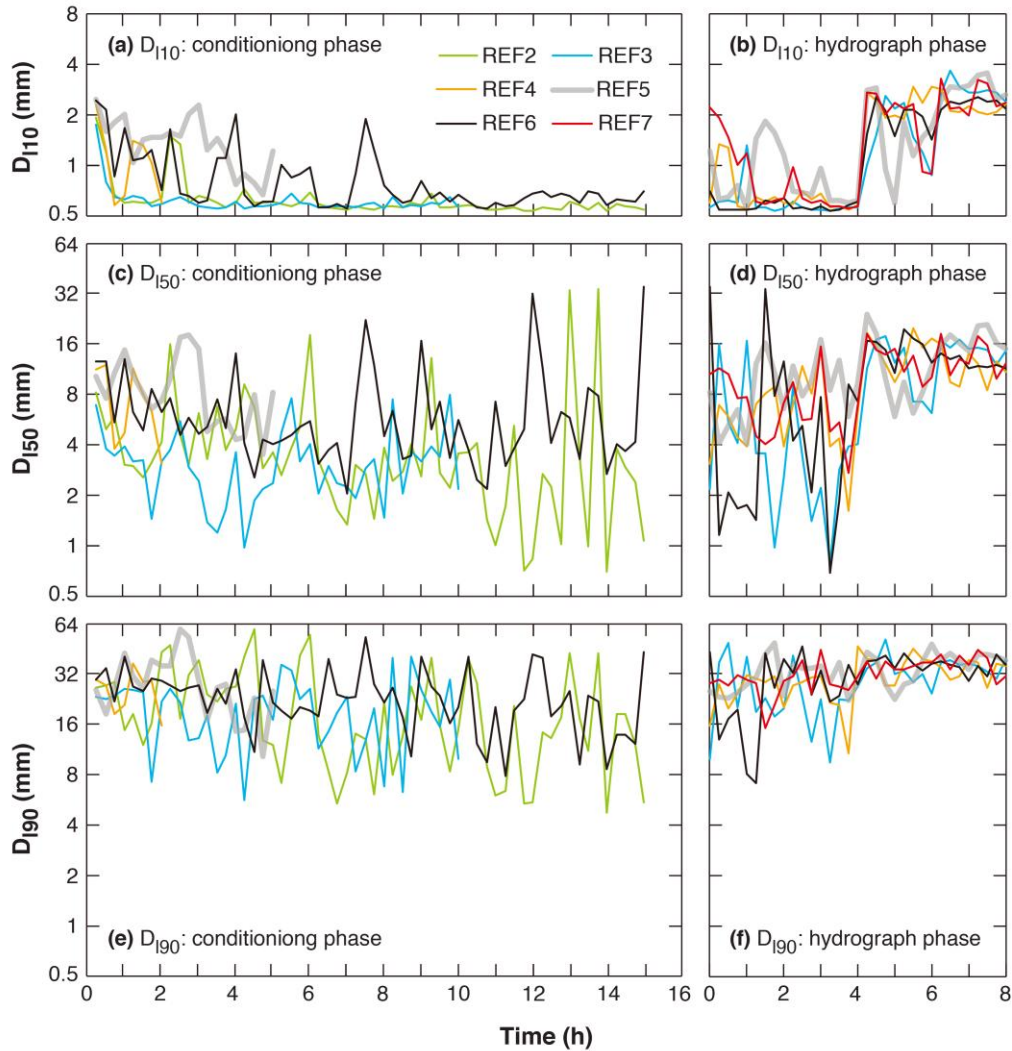
340
341 **Figure 7.** Sediment output measured at a trap during (a) the whole hydrograph; (b) Step 1 of the hydrograph; (c) Step
342 2 of the hydrograph; (d) Step 3 of the hydrograph; (e) Step 4 of the hydrograph.

343 However, if we study the sediment transport during each step of the hydrograph, we can find that in Step 1
344 REF7 (0.25) has much larger sediment output than the other experiments, as shown in Fig. 7(b). For Step 1, the
345 sediment output is 1.1 in REF6 (15), is 3.4~4.4 kg in REF4 (2) REF5 (5) and REF 3(10), and increases sharply to 23.4
346 kg in REF7 (0.25) (which is more than 20 times of that in REF6 (15)). This agrees with the results for instantaneous
347 sediment transport rate shown in Fig. 6(b), and shows that the duration of conditioning flow can influence the sediment
348 transport at the beginning of the subsequent flood, with a longer conditioning phase leading to less sediment transport.
349 When the duration of conditioning flow is over 2 hours, the subsequent sediment transport rate becomes rather
350 insensitive to further increase of conditioning duration, indicating that the reorganization of the river bed under
351 conditioning flow is mostly finished within 2 hours. The effects of stress history on subsequent sediment transport can
352 hardly be observed during Step 2 of the hydrograph (Fig. 7(c)). Sediment output in REF7 (0.25) reduces significantly
353 to similar magnitude of other experiments, because most of the loose bed material in REF7 (0.25) has been moved by
354 the end of Step 1. More specifically, the volumes of sediment output in this step ranges between 3.1 kg and 8.6 kg,
355 with the largest output occurring in REF5 (5) and the minimum output occurring in REF3 (10). We further calculate
356 the correlation coefficient between sediment output and conditioning duration and obtain a value of $r = -0.61$,
357 indicating that a longer conditioning duration can no longer lead to a larger sediment output in this step. In Step 3 of
358 the hydrograph (Fig. 7(d)), sediment output in REF7 (0.25) and REF4 (2) is larger than in other 3 experiments which
359 have longer conditioning phases. But in this step the sediment output in REF7 (0.25) is no more than three times that
360 of the sediment output in REF3 (10), which has the minimum sediment output. this-This difference of sediment output
361 among experiments is not as significant as in Step 1. In the last step of the hydrograph, with the flow discharge and
362 sediment supply approaching their peaks, the difference in sediment output among the five experiments again becomes
363 small, with the values ranging between 72.1 kg in REF4 (2) and 119.6 kg in REF6 (15). This demonstrates present
364 similar sediment outputs, demonstrating that little influence of stress history remains in this step.

365 Figure 8 shows the temporal variation of the grain size distribution of the bedload. Here D_{110} , D_{150} , and D_{190}
366 denote grain sizes such that 10%, 50%, and 90% are finer in the bedload, respectively. Accuracy of the measurements
367 is estimated by comparing the light table data with the trap data. Results show that for our experiments, the light table
368 method has good accuracy in terms of the median size of bedload (D_{150}), with an overestimation by 3% on average
369 (111 samples and a standard deviation of 40.1%). Measurements of D_{110} and D_{190} show less accuracy, with an
370 underestimation by 20% on average (111 samples and a standard deviation of 39.0%) for D_{110} and an overestimation
371 by 30% on average (111 samples and a standard deviation of 26.5%) for D_{190} . Details concerning of this uncertainty
372 analysis are presented in the Supporting Information.

373 The value of D_{110} shows a decreasing trend during the conditioning phase (Fig. 8 (a)), with a value of more
374 than 2 mm at the beginning to about 0.6 mm after 15 hours, in spite of the large fluctuations before 8 hours. The
375 decrease of D_{110} reflects an increase in the fraction of the finest sediment in bedload. In the first two steps of the
376 hydrograph (Fig. 8(b)), the value of D_{110} is relatively stable for experiments with long conditioning phases (i.e., REF6
377 (15) and REF3 (10)), but shows a decreasing trend along with fluctuations for experiments with short conditioning
378 phases (i.e., REF7 (0.25), REF4 (2), and REF5 (5)). The last two steps of the hydrograph see an evident increase in
379 the value of D_{110} compared with the first two steps, due to the increase of flow discharge and sediment supply (Fig.
380 8(b)). We note that such an increase in the D_{110} is larger than the standard deviation of measurements, as shown above.

381 Figures 8(c) and 8(d) show the temporal variation of D_{150} . Compared with that of D_{110} , the temporal variation
382 of D_{150} shows more significant fluctuations during the conditioning phase (especially after $t = 10$ hour), as well as at
383 the beginning of the hydrograph. ~~This can be shown by the coefficient of variation (cv) of the grain size. For the~~
384 ~~conditioning phase (after $t = 10$ hour), the cv of D_{110} show an average value of 0.05 whereas the cv of D_{150} show an~~
385 ~~average value of 1.44. For Step 1 of the hydrograph phase, the cv of D_{110} show an average value of 0.35 whereas the~~
386 ~~cv of D_{150} show an average value of 0.66. For Step 2 of the hydrograph phase, the cv of D_{110} show an average value of~~
387 ~~0.12 whereas the cv of D_{150} show an average value of 0.54. and a decreasing or increasing trend for grain size in the~~
388 ~~conditioning/hydrograph phase is not as evident.~~ As for the temporal variation of D_{190} (in Figs. 8(e) and 8(f)), the
389 fluctuations are still significant, with the average cv being 0.61, 0.34, 0.27 for the conditioning phase (after $t = 10$
390 hour), Step 1 of hydrograph phase, and Step 2 of hydrograph phase, respectively. ~~and Besides,~~ there is ~~almost~~ no
391 ~~significant increase of decrease of trend for D_{190} either increasing or decreasing grain size~~ during the experiment. This
392 indicates that the transport of the coarsest sediment is not sensitive to the variation of our experimental conditions.
393 The more significant fluctuations in D_{150} and D_{190} might be attributed to the fact that during relatively low flow coarse
394 sediment is more likely to be near the threshold of motion and move intermittently, e.g. ~~as individual grains in pulses,~~
395 as opposed to the more continuous movement for fine sediment. These fluctuations gradually diminish with the
396 increase of flow and sediment supply, as the static armor on bed surface transits to mobile armor and the movement
397 of coarse grains become more continuous.



398
 399 **Figure 8.** Temporal adjustments of characteristic grain sizes of bedload. (a) D_{110} during conditioning phase; (b) D_{110}
 400 during hydrograph phase; (c) D_{150} during conditioning phase; (d) D_{150} during hydrograph phase; (e) D_{190} during
 401 conditioning phase; (f) D_{190} during hydrograph phase.

402 With the fractional sediment transport rate measured by the light table, we also analyze the sediment mobility
 403 of each size range during the experiment. Results show that sediment transport rate is characterized by equal mobility
 404 (i.e., the GSD of sediment load matches the GSD of sediment on bed surface) at the beginning of the conditioning
 405 phase, but moves to partial/selective mobility after a relatively long conditioning phase as well as during the first two
 406 steps of the hydrograph. However, with the increase of flow discharge and sediment supply, the sediment transport
 407 regime gradually returns to equal mobility during the last two steps of the hydrograph. Details of the analysis are
 408 presented in the Supporting Information.

409 4 Discussion

410 4.1 Threshold of sediment motion in experiments

411 The threshold of sediment motion is a key parameter for the prediction of bedload transport. Previous studies
412 on the stress history effect often start with a conditioning flow that is below the threshold of motion, and then gradually
413 increase the flow discharge, so that the threshold of motion can be directly estimated in the experiment (e.g., Monteith
414 and Pender, 2005; Masteller and Finnegan, 2017; Ockelford et al., 2019; etc.). Because our experiments implement a
415 conditioning flow which can mobilize sediment (sediment transport at the beginning of the conditioning phase is
416 especially large), the threshold of motion cannot be observed directly in the experiment. Here we [follow the method
417 applied in Hassan et al. \(2020\), and](#) estimate the threshold of sediment motion [by adopting with](#) the Wong and Parker
418 (2006) sediment transport relation, which is a revision of the Meyer-Peter and Müller (1948) relation.

419 We use the Wong and Parker (2006) relation, which maintains the exponent 1.5, of Meyer-Peter and Muller
420 (1948):

$$421 \quad q_s^* = 3.97 \left(\tau_{s50}^* - \tau_c^* \right)^{1.5} \quad (1)$$

$$422 \quad q_s^* = \frac{q_s}{\sqrt{RgD_{s50} D_{s50}}} \quad (2)$$

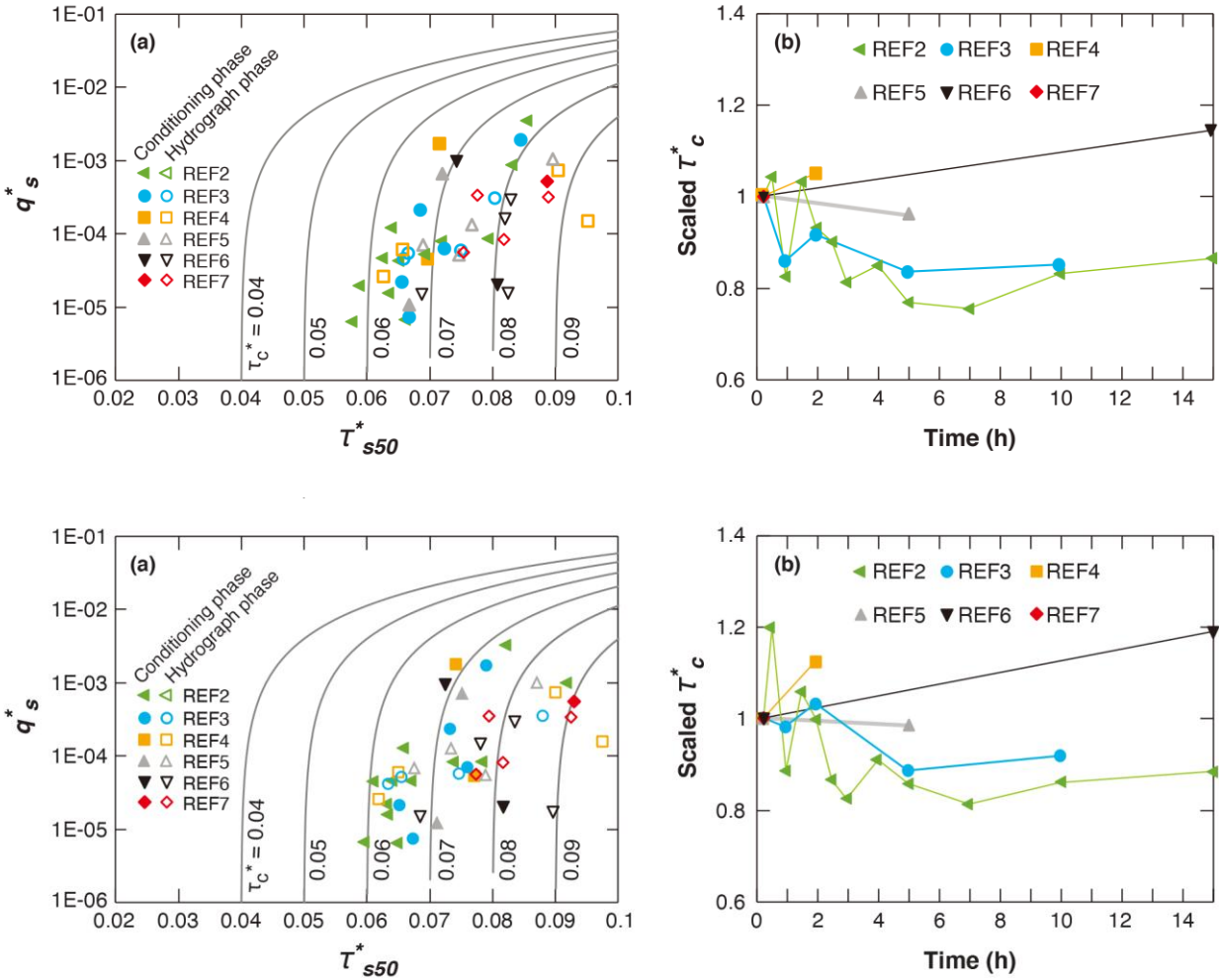
$$423 \quad \tau_{s50}^* = \frac{\tau_b}{\rho g R D_{s50}} \quad (3)$$

$$424 \quad \tau_b = \rho g h S_w \quad (4)$$

425 where q_s^* is the dimensionless bedload transport rate (Einstein number) defined by Eq. (2), τ_{s50}^* is the Shields number
426 for surface median grain size D_{s50} defined by Eq. (3), τ_b is the flow shear stress calculated using the depth-slope
427 product (Eq. (4)), τ_c^* is the critical Shields number for the threshold of sediment motion, q_s is the volumetric sediment
428 transport rate per unit width; h is water depth, S_w is water surface slope, $R = 1.65$ is the submerged specific gravity of
429 sediment, $g = 9.81 \text{ m/s}^2$ is the gravitational acceleration and $\rho = 1000 \text{ kg/m}^3$ is the water density. Wong and Parker
430 (2006) proposed a value of 0.0495 for τ_c^* in Eq. (1). Here we obtain q_s^* and τ_{s50}^* from the measured data of the
431 experiments, and back calculate the value of τ_c^* using Eq. (1). [It is worth mentioning that in Hassan et al. \(2020\) three
432 different methods, including the method as described above, are applied to estimate the threshold of sediment motion.
433 Estimation with the three different methods shows very similar temporal trend and variability.](#)

434 Figure 9(a) shows the values of q_s^* vs. τ_{s50}^* for each experiment, along with the Wong and Parker (2006) type
435 relation (Eq. (1)) with various values for τ_c^* (from 0.04 to 0.09). It can be seen from the figure that the measured
436 sediment transport [rate](#) is relatively low, with most points below the dimensionless value of 0.001. This indicates that
437 the Shields number in our experiment is slightly larger than the critical Shields number, a state that is typical for
438 gravel-bed rivers (Parker, 1978). The four points with dimensionless transport rate above 0.001 are all at the beginning

439 of the conditioning flow ($t = 15$ minutes). The values of q_s^* basically show an increasing trend with the increase of
 440 τ_{s50}^* , with the correlation coefficient between τ_{s50}^* and $\log(q_s^*)$ (in consistent with the semi-log scale of Figure 9(a))
 441 being 0.58. Besides, but with the values of critical Shields number τ_c^* shown in Figure 9(a) covers a rather wide range
 442 (from less than 0.06 to larger than 0.09).



443

444

445 **Figure 9.** (a) Dimensionless sediment transport rate q_s^* vs. Shields number τ_{s50}^* using surface median grain size for
 446 measured transport rates (points). Also shown are lines for the Wong and Parker (2006) type equation (Eq. 1) using
 447 different values for τ_c^* . (b) Temporal adjustment of scaled τ_c^* (τ_c^* over τ_c^* at 15 minutes) during the conditioning
 448 phase. Here τ_c^* is back-calculated using Eq. (1) (Wong and Parker (2006) type relation).

449 Table 2 shows the values of τ_c^* back-calculated at the beginning ($t = 15$ minutes) and the end of the
 450 conditioning phase in each experiment. The back-calculated values of τ_c^* vary in the range 0.0665-0.086090 for the
 451 conditioning phase, which is well above the value of 0.0495 as recommended by Wong and Parker (2006). Lamb et
 452 al. (2008) demonstrated that critical shear stress can become larger for large bed slope, and they proposed a relation
 453 which considers the effect of bed slope,

454 $\tau_c^* = 0.15S_b^{0.25}$ (5)

455 where S_b is bed slope. For comparison, Table 2 also shows the values of τ_c^* calculated by Eq. (5). Results shows that
 456 for the conditioning phase of our experiments, τ_c^* calculated by Eq. (5) is above 0.06, which is much higher than the
 457 recommended value of Wong and Parker (2006) ~~and is closer to the values back-calculated by Eq. (1)~~. Besides, the
 458 τ_c^* values predicted by the Lamb et al. (2008) relation show little variability among different experiments, compared
 459 with the values back-calculated with equation (1) based on experimental data. More specifically, the cv values are
 460 0.032 at $t = 15$ minutes and 0.031 at the end of the conditioning phase for τ_c^* predicted by Lamb et al. (2008) relation,
 461 but become 0.10 at $t = 15$ minutes and 0.12 at the end of the conditioning phase for τ_c^* back-calculated with equation
 462 (1) using measured data. Such discrepancies could be ascribed to the fact the relation of Lamb et al. (2008) considers
 463 only the influence of bed slope, but without considering the effects of other mechanisms like organization of surface
 464 texture, infiltration of fine particles, etc. These potential effects are discussed in more detail in Section 4.2, indicating
 465 that only the slope effect cannot explain the observed range of τ_c^* .

466 Here we also estimate the uncertainties associated with the calculation of τ_c^* . For the τ_c^* back-calculated
 467 with equation (1), ~~the~~ its global uncertainty is estimated by combining the uncertainties of each parameter ~~as~~ involved
 468 in the calculation, i.e. water depth h , water surface slope S_w , sediment transport rate q_s , and surface median grain size
 469 D_{s50} . The applied ranges of h and S_w are the measured values plus/minus the errors associated with the gauge point.
 470 The applied ranges of q_s and D_{s50} are the measured values plus/minus the standard deviations as reported in Section 3.
 471 Results of the uncertainties are presented in the brackets in Table 2. For the τ_c^* values calculated with ~~the~~ Equation
 472 (5), the uncertainties are only from the bed slope S_w (which is related with the resolution of point gauge), and is less
 473 than $\pm 1\%$ according to our ~~as we~~ estimates~~d~~. Therefore, the uncertainty~~ies~~ of τ_c^* calculated with the Equation (5) is
 474 not presented in the table. It can be seen from Table 2 that the values of τ_c^* calculated with the Equation (5) are mostly
 475 within the uncertainty range of τ_c^* back-calculated with Eq. (1), with the values closer to the lower bound of the
 476 uncertainty range.

477
 478 **Table 2.** Values of τ_c^* at the beginning ($t = 15$ minutes) and the end of conditioning phase in each experiment. Here
 479 τ_c^* is back-calculated with Eq. (1). Also shown here are values of τ_c^* estimated with the equation of Lamb et al. (2008)
 480 for comparison. Values in the brackets denote the range of uncertainty associated with the τ_c^* values back-calculated
 481 with Eq. (1).

| | | REF2 | REF6 | REF3 | REF5 | REF4 | REF7 |
|------------------------|----------------------------|-------|-------|-------|-------|-------|--------|
| | | (15) | (15) | (10) | (5) | (2) | (0.25) |
| t = 15 minutes | Back-calculated by Eq. (1) | 0.076 | 0.070 | 0.078 | 0.069 | 0.066 | 0.086 |
| | Lamb et al. (2008) | 0.063 | 0.066 | 0.061 | 0.065 | 0.061 | 0.066 |
| End of conditioning | Back-calculated by Eq. (1) | 0.066 | 0.081 | 0.067 | 0.066 | 0.069 | 0.086 |
| | Lamb et al. (2008) | 0.061 | 0.063 | 0.060 | 0.063 | 0.062 | 0.066 |

| | <u>$t = 15$ minutes</u> | | <u>End of conditioning</u> | |
|--------------------|---------------------------------------|---------------------------|---------------------------------------|---------------------------|
| | <u>Back-calculated by Eq. (1)</u> | <u>Lamb et al. (2008)</u> | <u>Back-calculated by Eq. (1)</u> | <u>Lamb et al. (2008)</u> |
| <u>REF2 (15)</u> | <u>0.073</u> <u>(0.064, 0.083)</u> | <u>0.063</u> | <u>0.065</u> <u>(0.057, 0.074)</u> | <u>0.061</u> |
| <u>REF6 (15)</u> | <u>0.068</u> <u>(0.053, 0.089)</u> | <u>0.066</u> | <u>0.081</u> <u>(0.072, 0.093)</u> | <u>0.063</u> |
| <u>REF3 (10)</u> | <u>0.073</u> <u>(0.061, 0.088)</u> | <u>0.061</u> | <u>0.067</u> <u>(0.058, 0.079)</u> | <u>0.060</u> |
| <u>REF5 (5)</u> | <u>0.072</u> <u>(0.061, 0.085)</u> | <u>0.065</u> | <u>0.071</u> <u>(0.062, 0.081)</u> | <u>0.063</u> |
| <u>REF4 (2)</u> | <u>0.068</u> <u>(0.059, 0.079)</u> | <u>0.061</u> | <u>0.077</u> <u>(0.066, 0.090)</u> | <u>0.062</u> |
| <u>REF7 (0.25)</u> | <u>0.090</u> <u>(0.075, 0.109)</u> | <u>0.066</u> | <u>0.090</u> <u>(0.075, 0.109)</u> | <u>0.066</u> |

483

484

485

486

487

488

489

490

491

492

493

494

495

496

497

In Fig. 9(b), we plot the scaled τ_c^* during the conditioning phase of our experiments. For each experiment, the scaled τ_c^* is calculated as the ratio between τ_c^* and the corresponding τ_c^* at $t = 15$ minutes. τ_c^* implemented here is back-calculated with Eq. (1). The scaled τ_c^* collapses on a value of unity at $t = 15$ minutes (i.e., the first point of each experiment). It can be seen from the figure that different trends are exhibited for the adjustment of τ_c^* from $t = 15$ minutes to the end of conditioning phase, with REF2 (15) and REF3 (10) exhibiting a decreasing trend, ~~REF4 (2)~~ and REF5 (5) exhibiting very slight changes, and ~~REF4 (2) and~~ REF6 (15) exhibiting an increasing trend. The decrease of τ_c^* in REF2 (15) and REF3 (10) is accompanied by a reduction of Shields number τ_{s50}^* , mainly due to the increase of surface median grain size D_{s50} . Moreover, the variation of back-calculated τ_c^* is mostly within a range of $\pm 20\%$, in agreement with our observation that variation of bed topography and bed surface texture become insignificant after 15 minutes. It should be noted that τ_c^* cannot be back-calculated using Eq. (1) within the first 15 minutes of the conditioning phase, since the information for flow depth, water surface slope and bed surface GSD is not available. Nevertheless, we expect the adjustment of τ_c^* could be evident within the first 15 minutes, since the adjustments of both bed topography and bed surface are significant during this period (as shown in Sect. 3.1).

498

4.2 Implications and limitations

499

500

501

502

503

504

505

506

Previous research has shown that antecedent conditioning flow can lead to an increased critical shear stress and reduced sediment transport rate during subsequent flood event (Hassan and Church, 2000; Haynes and Pender, 2007; Ockelford and Haynes, 2013; Masteller and Finnegan, 2017; etc.). Our flume experiments also show a ~~reduced~~ reduction in sediment transport rate, especially at the beginning of the hydrograph, in response to the implementation of antecedent conditioning flow (as shown in Fig. 6(b) and Fig. 7). However, our results are different from previous research in that the influence of antecedent conditioning flow is found to last for a relatively short time at the beginning of the following hydrograph, and then gradually diminish with the increase of flow intensity as well as sediment supply (Figs. 6 and 7). Such results indicate that increasing flow intensity and sediment supply during a

507 flood event can lead to the loss of memory of stress history. A similar phenomenon was observed by Mao (2018) in
508 his experiment, where sediment transport during a high-magnitude flood event was not much affected by the
509 occurrence of lower-magnitude flood event before. Besides, the subsequent hydrograph leads to evident bed
510 degradation (Fig. 3) and increase of sediment transport rate (Figs. 6 and 7), but does not lead to evident change of
511 surface texture or break of the armor layer (Fig. 5). This is in agreement with the observation of Ferrer-Boix and
512 Hassan (2015) during experiments of successive water pulses.

513 Our results have practical implications for mountain gravel bed rivers. The importance of conditioning flow
514 has long been discussed in the literature, and researchers have suggested that the stress history effect be considered in
515 the modeling and analysis of gravel bed rivers. For example, previous research states that existing sediment transport
516 theory for gravel bed rivers (e.g., Meyer-Peter and Müller, 1948; Wilcock and Crowe, 2003; Wong and Parker, 2006;
517 etc.) might lead to unrealistic predictions if the stress history effect is not taken into account (Masteller and Finnegan,
518 2017; Mao, 2018; Ockelford et al., 2019). Our results indicate that the stress history effect is important and needs to
519 be considered for low flow as well as the beginning of the flood event, but becomes insignificant as the flow gradually
520 approaches high flow discharge. ~~This could have implications in river engineering such as water and sediment~~
521 ~~regulation schemes for mountain gravel bed rivers.~~

522 To explain the effect of stress history, Ockelford and Haynes (2013) has summarized the following possible
523 mechanisms. (1) Vertical settling during the conditioning flow consolidates the bed into a tighter packing arrangement
524 which is more resistant to entrainment. (2) Local reorientation and rearrangement of surface particles provide a greater
525 degree of imbrication, less resistance to fluid flow, as well as direct sheltering on the bed surface. (3) The infiltration
526 of fines into low-relief pore spaces can further increase the bed compaction. In the experiment of Masteller and
527 Finnegan (2017), it was found that the most drastic changes during conditioning flow are manifest in the extreme tail
528 of the elevation distribution (i.e., the reorientation of the highest protruding grains into nearby available pockets) and
529 go therefore undetected in most bulk measurements (e.g. the mean bed elevation ~~or~~, standard deviation of bed
530 topography, or the bed surface GSD). They demonstrated that such reorganization of the highest protruding grains can
531 indeed lead to noticeable differences in the threshold of sediment transport (Masteller and Finnegan, 2017). This might
532 explain the observation in our experiment that after the first 15 minutes of the conditioning phase, adjustments of the
533 bed topography and the bed surface GSD become insignificant, but the sediment transport rate as well as its GSD
534 keeps adjusting consistently.

535 In our experiments as well as previous experiments that study the effect conditioning flow (e.g., Monteith
536 and Pender, 2005; Masteller and Finnegan, 2017; Ockelford et al., 2019; ~~ete~~), no sediment supply is implemented
537 during the conditioning flow, and the flow can reorganize the bed surface to a state that is more resistant to sediment
538 entrainment. Therefore, it is straightforward to expect that the conclusions based on our flume experiments to apply
539 for natural rivers where sediment supply is relatively low during low flow conditions. However, some gravel-bed
540 rivers have quite active hillslopes, and sediment input from hillslopes to river channel can occur regularly (Turowski
541 et al., 2011; Reid et al., 2019). Since the sediment material from hillslopes is typically loose and easy to transport,
542 under such circumstances a long inter-event duration (i.e., low-flow duration) might lead to an enhanced sediment
543 transport rate in the subsequent flood (Turowski et al., 2011).

544 It should also be noted that in previous experiment on the stress history effect, conditioning flow is often set
545 below the threshold of sediment motion. One exception is the experiment of Haynes and Pender (2007) in which the
546 conditioning flow ~~is was~~ above the threshold of motion for D_{50} . ~~By implementing conditioning flow with various~~
547 ~~durations and magnitudes, they demonstrated that a longer~~ duration of conditioning flow will increase the bed stability
548 ~~whereas a higher magnitude of conditioning flow will reduce the bed stability. However, since the subsequent flow~~
549 ~~they implement to test the bed stability was constant through time, their results did not show how a subsequent flow~~
550 ~~event with increasing intensity would affect the stress history. In this the present paper~~ Here we ~~also~~ implement a
551 conditioning flow which can mobilize sediment, especially at the beginning of the conditioning phase during which
552 evident sediment transport occurs. ~~Moreover, by implementing a subsequent (rising limb of) the hydrograph, we find~~
553 ~~that the stress history can persist during the beginning of the hydrograph but is eventually erased out as the flow~~
554 ~~intensity increases goes large. In our experiments, we varied the duration of conditioning flow by fixing the~~
555 ~~conditioning flow magnitude. In this sense, how the stress history formed under various magnitudes of conditioning~~
556 ~~flow (both above-and below-threshold) would be affected by a subsequent hydrograph still merits future~~
557 ~~research. Compared with the below threshold conditioning flow, we consider that the above threshold conditioning~~
558 ~~flow can induce more evident reorganization of bed surface, which might be more lasting during subsequent flood.~~
559 ~~That said, we expect the conclusion of this study can still hold if below threshold conditioning flow is implemented.~~
560 ~~Nevertheless, flume experiments with various magnitudes of conditioning flow (both above and below threshold of~~
561 ~~motion) merit future study.~~

562 ~~Recently, Church et al. (2020) drew attention to the reproducibility of results in geomorphology. They~~
563 ~~distinguished three levels of “reproducibility”, including “repetition”, “replication”, and “reproduction”. In this paper,~~
564 ~~the repetition of the experimental results is tested by repeating the conditioning phase with the longest duration (REF6~~
565 ~~(15) and REF2 (15)). The two experiments show similar results during the conditioning phase in terms of standard~~
566 ~~deviation of bed elevation, GSD of bed surface, sediment transport rate, and GSD of sediment load. However, the~~
567 ~~reproduction of the experimental results, which requires independent tests undertaken using different materials and/or~~
568 ~~different conditions of measurement, and which is more significant, according to Church et al. (2020), for advancing~~
569 ~~of the science according to Church et al. (2020), has not been tested in this paper. In this regard, more efforts are~~
570 ~~needed in future study to test the reproducibility of the conclusions given in this paper. Besides, considering that the~~
571 ~~conditions of existing experiments on stress history effect are limited, implementation of numerical simulations under~~
572 ~~a wider range of conditions also merits future study.~~

573 **5 Conclusions**

574 In this paper, the effect of antecedent conditioning flow (i.e., the effect of stress history) on the
575 morphodynamics of gravel-bed rivers during subsequent floods is studied via flume experimentation. The experiment
576 described here is designed based on the conditions of East Creek, Canada. The experiment consisteds of two phases:
577 a conditioning phase with constant water discharge and no sediment supply, followed by a hydrograph phase with
578 hydrograph and sedimentograph. Five runs (REF 3~7) were conducted with identical experimental conditions except
579 different durations of conditioning phase. Another run (REF 2), which consisteds of only the conditioning phase, is

580 conducted in order to test the reproducibility of experimental results during the conditioning flow. Experimental results
581 show the following.

- 582 ● Adjustments of channel morphology (including channel bed longitudinal profile, standard deviation of bed
583 elevation, characteristic grain sizes of bed surface material) are evident during the first 15 minutes of the
584 conditioning phase, but become insignificant during the remainder of the conditioning phase.
- 585 ● The implementation of conditioning flow can indeed lead to a reduction in sediment transport during the
586 subsequent hydrograph, which agrees with previous research.
- 587 ● However, the effect of stress history on sediment transport rate is limited to a relatively short time at the beginning
588 of the hydrograph, and gradually diminishes with the increase of flow discharge and sediment supply, indicating
589 a loss of memory of stress history under high flow discharge. Also, the effect of stress history on the GSD of
590 both bed surface and bedload is not evident.
- 591 ● The threshold of sediment motion is estimated with the form of the Wong and Parker (2006) relation. The
592 estimated critical Shields number varies in the range 0.066~0.086 during the conditioning phase (excluding the
593 first 15 minutes), and is higher than the value recommended by Wong and Parker (2006).

594 Our study has implications in regard to a wide range of issues for mountain gravel-bed rivers, including
595 sediment budget analysis, river morphodynamic modeling, water and sediment regulation, flood management, and
596 ecological restoration schemes.

597 **Notation**

598 D_{150} : grain size such that 50 percent in sediment load is finer (similarly D_{110} is such that 10 percent in sediment load
599 is finer and D_{190} is such that 90 percent in sediment load is finer).

600 D_{s50} : grain size such that 50 percent on bed surface is finer (similarly D_{s10} is such that 10 percent on bed surface is
601 finer and D_{s90} is such that 90 percent on bed surface is finer).

602 F_r : Froude number.

603 g : gravitational acceleration.

604 h : water depth.

605 Q_s : sediment transport rate.

606 q_s : volumetric sediment transport rate per unit width.

607 q_s^* : the dimensionless bedload transport rate (Einstein number).

608 R : submerged specific gravity of sediment.

609 S_b : bed slope.

610 S_w : water surface slope.

611 ρ : water density.

612 Δz_b : mean difference of bed elevation;

613 τ_b : bed shear stress.

614 τ_c^* : critical Shields number for the threshold of sediment motion.

615 τ_{s50}^* : dimensionless shear stress (Shields number) of the D_{s50} .

616 **Data availability**

617 Data used for the analysis can be found at doi: 10.6084/m9.figshare.12758414 (An, 2020).

618 **Author contribution**

619 Marwan A. Hassan and Xudong Fu designed the research. Carles Ferrer-Boix performed the experiments. Chenge An
620 processed and analyzed the experimental data. Chenge An prepared the manuscript with contributions from all
621 coauthors.

622 **Competing interests**

623 The authors declare that they have no conflict of interest.

624 **Acknowledgments**

625 Gary Parker provided constructive comments and helped edit ~~of~~ this paper. Maria A. Elgueta-Astaburuaga
626 helped conduct the experiments. Rick Ketler provided support in equipment and data collections. Eric Leinberger
627 provided support in designing the figures. We thank Jens Turowski and another anonymous reviewer for their
628 constructive comments, which helped us greatly improve the paper. The participation of Chenge An was supported
629 by grant from China Postdoctoral Science Foundation (grant 2018M641368). The participation of Xudong Fu was
630 supported by grants from the National Natural Science Foundation of China (grants 51525901 and 91747207).

631 **References**

632 An, C.: Experimental data on sediment transport and channel adjustment in a gravel-bed river: stress history effect,
633 doi: 10.6084/m9.figshare.12758414, 2020.

634 Carling, P. A., Kelsey, A., and Glaister, M. S.: Effect of bed roughness, particle shape and orientation on initial motion
635 criteria, in: Dynamics of Gravel-bed Rivers, edited by: Billi, P., Hey, R. D., Thorne, C. R., and Tacconi, P.,
636 John Wiley & Sons, Chichester, UK, 23-39, 1992.

637 Chartrand, S. M., Jellinek, A. M., Hassan, M. A., and Ferrer-Boix, C.: Morphodynamics of a width-variable gravel
638 bed stream: New insights on pool-riffle formation from physical experiments, Journal of Geophysical
639 Research-Earth Surface, 123(11), 2735-2766, <https://doi.org/10.1029/2017JF004533>, 2018.

640 Chen, X., Hassan, M. A., An, C., and Fu, X.: Rough correlations: Meta-analysis of roughness measures in gravel bed
641 rivers, Water Resources Research, 56, e2020WR027079, <https://doi.org/10.1029/2020WR027079>, 2020.

642 Chin, A., Anderson, S., Collison, A., Ellis-Sugai, B. J., Haltiner, J. P., Hogervorst, J. B., Kondolf, G. M., O'Hirok, L.
643 S., Purcell, A. H., Riley, A. L., and Wohl E.: Linking theory and practice for restoration of step-pool streams,
644 *Environmental Management*, 43, 645–661, doi:10.1007/s00267-008-9171-x, 2009.

645 [Church, M., Dudill, A., Venditti, J. G., and Frey, P.: Are Results in Geomorphology Reproducible? *Journal of*](#)
646 [Geophysical Research-Earth Surface](#), 125(8), e2020JF005553, <https://doi.org/10.1029/2020JF005553>, 2020.

647 [Curran, J. C., and Wilcock, P. R.: Effect of sand supply on transport rates in a gravel-bed channel, *Journal of Hydraulic*](#)
648 [Engineering](#), 131(11), 961–967, [https://doi.org/10.1061/\(ASCE\)0733-9429\(2005\)131:11\(961\)](https://doi.org/10.1061/(ASCE)0733-9429(2005)131:11(961)), 2005.

649 Elgueta-Astaburuaga, M. A., and Hassan, M. A.: Experiment on temporal variation of bed load transport in response
650 to changes in sediment supply in streams, *Water Resources Research*, 53, 763–778,
651 doi:10.1002/2016WR019460, 2017.

652 Ferrer-Boix, C. and Hassan, M. A.: Influence of the sediment supply texture on morphological adjustments in gravel-
653 bed rivers, *Water Resources Research*, 50(11), 8868–8890, doi:10.1002/2013WR015117, 2014.

654 Ferrer-Boix, C., and Hassan, M. A.: Channel adjustments to a succession of water pulses in gravel bed rivers, *Water*
655 *Resources Research*, 51, 8773–8790, doi:10.1002/2015WR017664, 2015.

656 Gomez, B. and Church, M.: An assessment of bed load sediment transport formulae for gravel rivers, *Water Resources*
657 *Research*, 25, 1161–1186, doi:10.1029/WR025i006p01161, 1989.

658 Hassan, M. A., and Church, M.: Experiments on surface structure and partial sediment transport on a gravel bed,
659 *Water Resources Research*, 36, 1885–1895, 2000.

660 Haynes, H., and Pender, G.: Stress history effects on graded bed stability, *Journal of Hydraulic Engineering*, 33, 343–
661 349, 2007.

662 Howard, A.: A detachment-limited model of drainage basin evolution, *Water Resources Research*, 30(7), 2261–2285,
663 1994.

664 Johnson, J. P. L.: Gravel threshold of motion: A state function of sediment transport disequilibrium? *Earth Surface*
665 *Dynamics*, 4(3), 685–703, <https://doi.org/10.5194/esurf-4-685-2016>, 2016

666 Klingeman, P. C., and Emmett, W. W.: Gravel bedload transport processes, in: *Gravel-Bed Rivers*, edited by: Hey, R.
667 D., Bathurst, J. C., and Thorne, C., John Wiley & Sons, Chichester, UK, 141–180, 1982.

668 Lamb, M. P., Dietrich, W. E., and Venditti, J. G.: Is the critical Shields stress for incipient sediment motion dependent
669 on channel-bed slope? *Journal of Geophysical Research-Earth Surface*, 113, F02008,
670 doi:10.1029/2007JF000831, 2008.

671 [Lenzi, M. A.: Step-pool evolution in the Rio Cordon, northeastern Italy, *Earth Surface Processes and Landforms*, 26,](#)
672 [991–1008, <https://doi.org/10.1002/esp.239>, 2001.](#)

673 Mao, L.: The effects of flood history on sediment transport in gravel bed rivers, *Geomorphology*, 322, 192–205,
674 <https://doi.org/10.1016/j.geomorph.2018.08.046>, 2018.

675 Marston, R. A.: Land, life, and environmental change in mountains, *Annals of the Association of American*
676 *Geographers*, 98, 507–520, <https://doi.org/10.1080/00045600802118491>, 2008.

677 Masteller, C. C., and Finnegan, N. J.: Interplay between grain protrusion and sediment entrainment in an experimental
678 flume, *Journal of Geophysical Research-Earth Surface*, 122, 274–289,
679 <https://doi.org/10.1002/2017GL076747>, 2017.

680 Masteller, C. C., Finnegan, N. J., Turowski, J. M., Yager, E. M., and Rickermann, D.: History dependent threshold
681 for motion revealed by continuous bedload transport measurements in a steep mountain stream, *Geophysical*
682 *Research Letters*, 46, 2583–2591, 2019.

683 Monteith, H., and Pender, G.: Flume investigation into the influence of shear stress history, *Water Resources Research*,
684 41, W12401, <https://doi.org/10.1029/2005WR004297>, 2005.

685 Montgomery, D. R., and Buffington, J. M.: Channel - reach morphology in mountain drainage basins, *Geological*
686 *Society of America Bulletin*, 109(5), 596–611, [https://doi.org/10.1130/0016-7606\(1997\)109<0596:CRMIMD>2.3.CO;2](https://doi.org/10.1130/0016-7606(1997)109<0596:CRMIMD>2.3.CO;2), 1997.

688 Montgomery, D. R., Buffington, J. M., Peterson, N. P., Schuett-Hames, D., and Quinn, T. P.: Stream-bed scour, egg
689 burial depths, and the influence of salmonid spawning on bed surface mobility and embryo survival, *Canadian*
690 *Journal of Fisheries and Aquatic Sciences*, 53, 1061–1070, 1996.

691 Meyer-Peter, E., and Müller, R.: Formulas for bed-load transport, in: *Proceedings of the 2nd Congress of International*
692 *Association for Hydraulic Structures Research*, Stockholm, Sweden, 7-9 June 1948, 39-64, 1948.

693 Ockelford, A., and Haynes, H.: The impact of stress history on bed structure, *Earth Surface Processes and Landforms*,
694 38, 717–727, <https://doi.org/10.1002/esp.3348>, 2013.

695 Ockelford, A., Woodcock, S., and Haynes, H.: The impart of inter-flood duration on non-cohesive sediment bed
696 stability, *Earth Surface Processes and Landforms*, 44, 2861-2871, doi:10.1002/esp.4713, 2019.

697 Paola, C., Heller, P. L., and Angevine, C. L.: The large-scale dynamics of grain-size variation in alluvial basins, I:
698 *Theory*, *Basin Research*, 4, 73–90, 1992.

699 Papangelakis, E., and Hassan, M. A.: The role of channel morphology on the mobility and dispersion of bed sediment
700 in a small gravel-bed stream, *Earth Surface Processes and Landforms*, 41, 2191–2206, 2016.

701 Paphitis, D., and Collins, M. B.: Sand grain threshold, in relation to bed stress history: an experimental study,
702 *Sedimentology*, 52, 827–838, 2005.

703 Parker, G.: Self-formed straight rivers with equilibrium banks and mobile bed. Part 2. The gravel river, *Journal of*
704 *Fluid Mechanics*, 89, 127-146, 1978.

705 Parker, G.: 1D sediment transport morphodynamics with applications to rivers and turbidity currents, available at:
706 http://hydrolab.illinois.edu/people/parkerg//morphodynamics_e-book.htm, 2004.

707 Powell, D. M., Reid, I., and Laronne, J. B.: Hydraulic interpretation of crossstream variations in bed-load transport,
708 *Journal of Hydraulic Engineering*, 125, 1243–1252, 1999.

709 Reid, D. A., Hassan, M. A., Bird, S., and Hogan D.: Spatial and temporal patterns of sediment storage over 45 years
710 in Carnation Creek, BC, a previously glaciated mountain catchment, *Earth Surface Processes and Landforms*,
711 44, 1584-1601, doi: 10.1002/esp.4595, 2019.

712 Reid, I., and Frostick, L. E.: Particle interaction and its effects on the thresholds of initial and final bedload motion in
713 coarse alluvial channels, in: *Sedimentology of Gravels and Conglomerates-Memoir 10*, edited by: Koster, E.
714 H., and Steel, R. J., Canadian Society of Petroleum Geologists, Calgary, Canada, 61–68, 1984.

715 Reid, I., Frostick, L. E., and Layman, J. T.: The incidence and nature of bedload transport during flood flows in coarse-
716 grained alluvial channels, *Earth Surface Processes and Landforms*, 10, 33–44, 1985.

717 Rickenmann, D.: Comparison of bed load transport in torrents and gravel bed streams, *Water Resources Research*, 37,
718 3295–3305, doi:10.1029/2001WR000319, 2001.

719 Schneider, J. M., Rickenmann, D., Turowski, J. M., Bunte, K., and Kirchner, J. W.: Applicability of bed load transport
720 models for mixed-size sediments in steep streams considering macro-roughness, *Water Resources Research*,
721 51, 5260–5283, doi:10.1002/2014wr016417, 2015.

722 Sklar, L., and Dietrich W. E.: A mechanistic model for river incision into bedrock by saltating bed load, *Water*
723 *Resources Research*, 40, W06301, doi:10.1029/2003WR002496, 2004.

724 Turowski, J. M., Yager, E. M., Badoux, A., Rickenmann, D., and Molnar, P.: The impact of exceptional events on
725 erosion, bedload transport and channel stability in a step-pool channel, *Earth Surface Processes and*
726 *Landforms*, 34, 1661-1673, <https://doi.org/10.1002/esp.1855>, 2009.

727 Turowski, J. M., Badoux, A., and Rickenmann, D.: Start and end of bedload transport in gravel-bed streams,
728 *Geophysical Research Letters*, 38, L04401, <https://doi.org/10.1029/2010GL046558>, 2011.

729 Venditti, J. G., Dietrich, W. E., Nelson, P. A., Wydzga, M. A., Fadde, J., and Sklar, L.: Mobilization of coarse surface
730 layers in gravel-bedded rivers by finer gravel bed load, *Water Resources Research*, 46, W07506,
731 <https://doi.org/10.1029/2009WR008329>, 2010.

732 Whiting, P. J., and Dietrich, W. E.: Boundary shear stress and roughness over mobile alluvial beds, *Journal of*
733 *Hydraulic Engineering*, 116, 1495–1511, 1990.

734 Wilcock, P. R., and Crowe, J. C.: Surface-based transport model for mixed-size sediment, *Journal of Hydraulic*
735 *Engineering-ASCE*, 129, 120–128, doi:10.1061/(asce)0733-9429(2003)129:2(120), 2003.

736 Wilcock, P. R., Kenworthy, S. T., and Crowe, J. C.: Experimental study of the transport of mixed sand and gravel,
737 *Water Resources Research*, 37(12), 3349–3358, 2001.

738 Wong, M., and Parker, G.: Reanalysis and correction of bed-load relation of Meyer-Peter and Müller using their own
739 database, *Journal of Hydraulic Engineering-ASCE*, 132, 1159–1168, doi:10.1061/(ASCE)0733-
740 9429(2006)132:11(1159), 2006.

741 Yager, E. M., Turowski, J. M., Rickenmann, D., and McArdeell, B. W.: Sediment supply, grain protrusion, and bedload
742 transport in mountain streams, *Geophysical Research Letters*, 39, L10402,
743 <https://doi.org/10.1029/2012GL051654>, 2012.

744 Zimmermann, A., Church, M., and Hassan, M. A.: Video-based gravel transport measurements with a flume mounted
745 light table, *Earth Surface Processes and Landforms*, 33(14), 2285-2296, <https://doi.org/10.1002/esp.1675>,
746 2008.